Multiple pathways to herbivory underpinned deep divergences in ornithischian evolution

Button, David; Porro, Laura; Lautenschlager, Stephan; Jones, Marc; Barrett, Paul

DOI:
10.1016/j.cub.2022.12.019

Document Version
Publisher's PDF, also known as Version of record

Citation for published version (Harvard):
Button, D, Porro, L, Lautenschlager, S, Jones, M & Barrett, P 2023, 'Multiple pathways to herbivory underpinned deep divergences in ornithischian evolution', *Current Biology*, vol. 33, no. 3, pp. 557-565.E7. https://doi.org/10.1016/j.cub.2022.12.019

Report

Current Biology

Multiple pathways to herbivory underpinned deep divergences in ornithischian evolution

Highlights

- The performance of the feeding apparatus is compared among key ornithischian taxa
- Diverse morphofunctional patterns are observed among early members of major clades
- These differences reveal distinct solutions to herbivory in each of these clades
- This non-convergence demonstrates that evolution is not necessarily predictable

Authors

David J. Button, Laura B. Porro, Stephan Lautenschlager, Marc E.H. Jones, Paul M. Barrett

Correspondence

david.button@bristol.ac.uk

In brief

Button et al. perform biomechanical modeling of the skull of early members of herbivorous ornithischian dinosaur clades. Their results demonstrate performance differences and distinct solutions to herbivory among taxa. These non-convergent responses to common ecological pressures highlight the potential unpredictability of morphological evolution.

Button et al., 2023, Current Biology *33*, 557–565
February 6, 2023
https://doi.org/10.1016/j.cub.2022.12.019

CellPress

Current Biology

CellPress
OPEN ACCESS

Report

Multiple pathways to herbivory underpinned deep divergences in ornithischian evolution

David J. Button,[1,4,5,*] Laura B. Porro,[2] Stephan Lautenschlager,[3] Marc E.H. Jones,[1] and Paul M. Barrett[1]
[1]Science Group, The Natural History Museum, Cromwell Road, London SW7 5BD, UK
[2]Centre for Integrative Anatomy, Department of Cell and Developmental Biology, University College London, Gower Street, London WC1E 6DE, UK
[3]School of Geography, Earth and Environmental Sciences, University of Birmingham, Birmingham B15 2TT, UK
[4]Present address: Bristol Palaeobiology Group, School of Earth Sciences, University of Bristol, Bristol BS8 1TQ, UK
[5]Lead contact
*Correspondence: david.button@bristol.ac.uk
https://doi.org/10.1016/j.cub.2022.12.019

SUMMARY

The extent to which evolution is deterministic is a key question in biology,[1–9] with intensive debate on how adaptation[6,10–13] and constraints[14–16] might canalize solutions to ecological challenges.[4–6] Alternatively, unique adaptations[1,9,17] and phylogenetic contingency[1,3,18] may render evolution fundamentally unpredictable.[3] Information from the fossil record is critical to this debate,[1,2,11] but performance data for extinct taxa are limited.[7] This knowledge gap is significant, as general morphology may be a poor predictor of biomechanical performance.[17,19,20] High-fiber herbivory originated multiple times within ornithischian dinosaurs,[21] making them an ideal clade for investigating evolutionary responses to similar ecological pressures.[22] However, previous biomechanical modeling studies on ornithischian crania[17,23–25] have not compared early-diverging taxa spanning independent acquisitions of herbivory. Here, we perform finite-element analysis on the skull of five early-diverging members of the major ornithischian clades to characterize morphofunctional pathways to herbivory. Results reveal limited functional convergence among ornithischian clades, with each instead achieving comparable performance, in terms of reconstructed patterns and magnitudes of functionally induced stress, through different adaptations of the feeding apparatus. Thyreophorans compensated for plesiomorphic low performance through increased absolute size, heterodontosaurids expanded jaw adductor muscle volume, ornithopods increased jaw system efficiency, and ceratopsians combined these approaches. These distinct solutions to the challenges of herbivory within Ornithischia underpinned the success of this diverse clade. Furthermore, the resolution of multiple solutions to equivalent problems within a single clade through macroevolutionary time demonstrates that phenotypic evolution is not necessarily predictable, instead arising from the interplay of adaptation, innovation, contingency, and constraints.[1–3,7–9,18]

RESULTS

Bite forces and functionally induced stresses were calculated via finite-element analysis (FEA) of the skulls of five early-diverging representatives from major ornithischian clades (the heterodontosaurid *Heterodontosaurus*, the putative thyrephoran or early-diverging ornithischian *Lesothosaurus*, the thyreophoran *Scelidosaurus*, the ornithopod *Hypsilophodon*, and the ceratopsian *Psittacosaurus*; Figure 1). Skull models were reconstructed from CT scans (Data S1), with retrodeformation procedures[26] applied to correct taphonomic damage and loaded with forces calculated through reconstruction of the jaw adductor muscle musculature from osteological correlates[27] (Figures 2 and S1; Tables S1–S3; STAR Methods).

Jaw musculature and bite performance

Lowest predicted bite forces occurred in *Lesothosaurus*, but substantial variance in absolute bite forces is observed among the other taxa (Tables S4 and S5). Nevertheless, comparable magnitudes are observed in similarly sized taxa (e.g., *Heterodontosaurus* and *Hypsilophodon*; Figure 2A). Comparison of biting efficiency (the mechanical advantage, as measured by the ratio of input muscle force to output bite force; Figure 2B) to the reconstructed sizes of the jaw adductor musculature (Figures 2C and 2D; Table S1) reveals striking differences among taxa. The lowest mechanical advantage values, at every biting position, were observed in *Heterodontosaurus*, with relatively low values also predicted across the toothrow in *Lesothosaurus* and *Scelidosaurus* (Figure 2B). Nevertheless, *Heterodontosaurus* achieved elevated bite forces through larger adductor muscles relative to skull size (Figure 2D), and *Scelidosaurus* achieved similar forces due to its greater overall body size, which is associated with absolutely larger (Figure 2C)—although relatively smaller (Figure 2D)—jaw adductors compared with other taxa.

In contrast to *Scelidosaurus* and *Heterodontosaurus*, greater efficiency, especially during posterior bites, was predicted in the

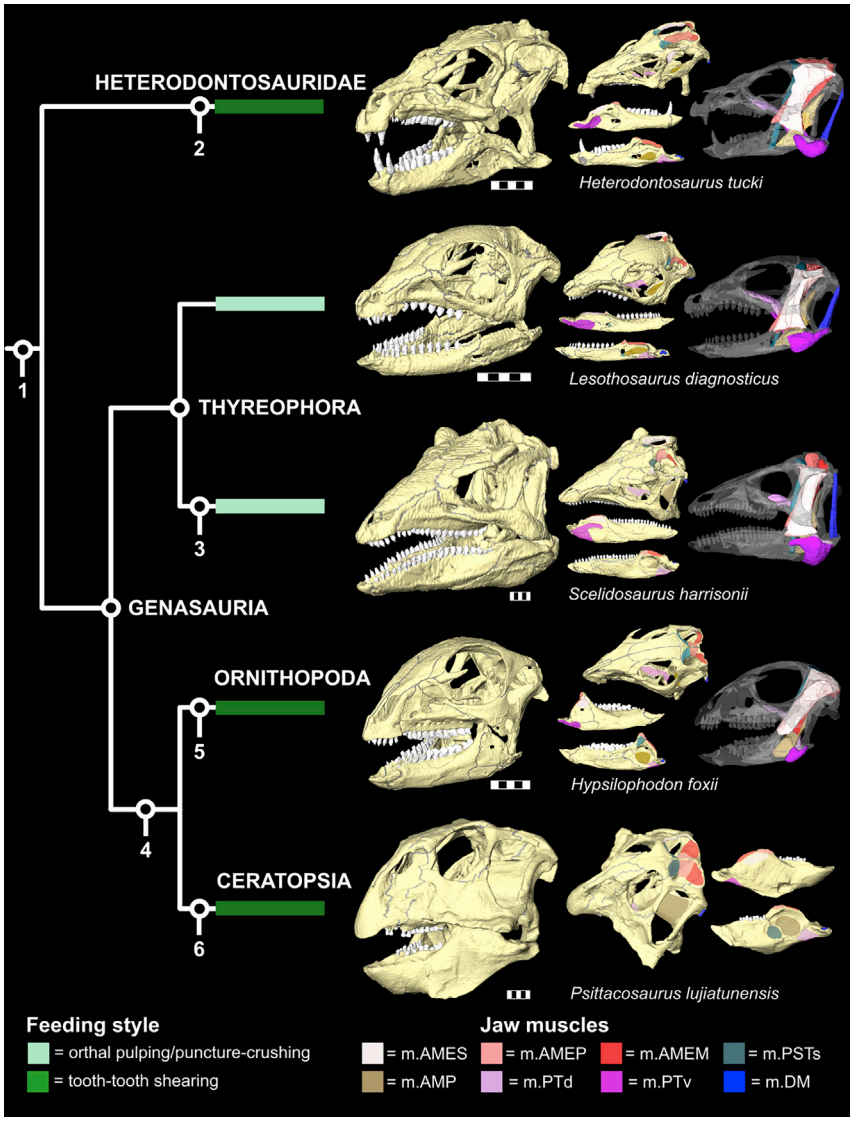

Figure 1. Reconstructed cranial osteology and myology of ornithischian taxa

Retrodeformed skulls of *Heterodontosaurus tucki*, *Lesothosaurus diagnosticus*, *Scelidosaurus harrisonii*, *Hypsilophodon foxii*, and *Psittacosaurus lujiatunensis*, with mapped origination and insertion areas, and reconstructed volumes of jaw muscles indicated. Scale bars for complete skulls, 20 mm. Skulls are mapped onto ornithischian phylogeny following.[82] Broad feeding style—orthal pulping/puncture crushing, with no systematic tooth-tooth occlusion vs. systematic tooth-tooth shearing across the toothrow—and characters of the feeding apparatus were also mapped onto this phylogeny. Characters of the feeding apparatus for numbered clades are as follows. (1) Ornithischia: predentary beak, subtriangular and denticulate tooth crowns, and orthal pulping/puncture crushing. (2) Heterodontosauridae: heterodont dentition and diastema, Heterodontosaurinae: tooth-tooth occlusion, asymmetrical tooth enamel, and hypsodont dentition,[49] increased relative size of adductor musculature. (3) Thyreophoroidea: increased body size. (4) Cerapoda: increase in size of temporal muscles (external adductors and pseudotemporalis groups) relative to the palatal musculature.[62] (5) Ornithopoda: increased height of coronoid process, posterior extension of toothrow medial to coronoid process, tooth-tooth occlusion, asymmetric tooth enamel,[34] and increased biting efficiency and relative bite force. (6) Ceratopsia: rostral bone, increased height of coronoid process, posterior extension of toothrow medial to coronoid process,[41] tooth-tooth occlusion, asymmetric tooth enamel,[83] increased adductor muscle size, increased robusticity of cranium and mandible, increased biting efficiency, and relative and absolute bite force. See Figure S1 for more information on adductor muscle reconstruction.

cerapodans *Hypsilophodon* and *Psittacosaurus* through a combination of structural modifications to the skull (increased height of coronoid process, extension of toothrow posterior to coronoid process, shortened snout; Figure 1) and jaw adductor musculature (greater relative contribution of the more mechanically advantageous external adductors compared with the palatal muscles; Figures 2C and 2D). Nevertheless, significant functional differences occurred between these two taxa: *Psittacosaurus* exhibited substantially greater absolute and relative jaw adductor forces (Figures 2C and 2D) and greater mechanical advantage at anterior biting positions, whereas more efficient bites at the posterior end of the toothrow are predicted in *Hypsilophodon* (Figure 2B).

Functionally induced stress

When scaled to absolute size, FEA revealed similar functionally induced stress magnitudes between all taxa during simulated bites (Figure 3), as expected given the general conservation of safety factors across vertebrates.[28] However, scaling to account for differences in size and applied force[29] (STAR Methods) revealed differences in relative performance between taxa (Figures 4 and S2). The lowest stress magnitudes, in both the cranium and mandible, were observed during simulated biting in *Psittacosaurus*. Patterns of relative stress distribution within the mandible were broadly similar between *Lesothosaurus* and *Hypsilophodon*, and the mandible of *Heterodontosaurus* exhibited lower overall magnitudes relative to these taxa (Figure 4). The mandible of *Scelidosaurus* behaved similarly for bites at the posterior dentition, but was relatively weaker than the other taxa, for its size, at more anterior biting positions, as indicated by large regions of elevated stress throughout the thin exterior walls of the dentary (Figure 4). By contrast, patterns of biting-induced stress within the cranium were consistent between all taxa, potentially reflecting the greater number of competing functional demands on the morphology of the cranium beyond those associated with feeding.[30]

DISCUSSION

Herbivory poses particular challenges for vertebrates,[31] and ornithischians exhibited numerous specializations of the feeding

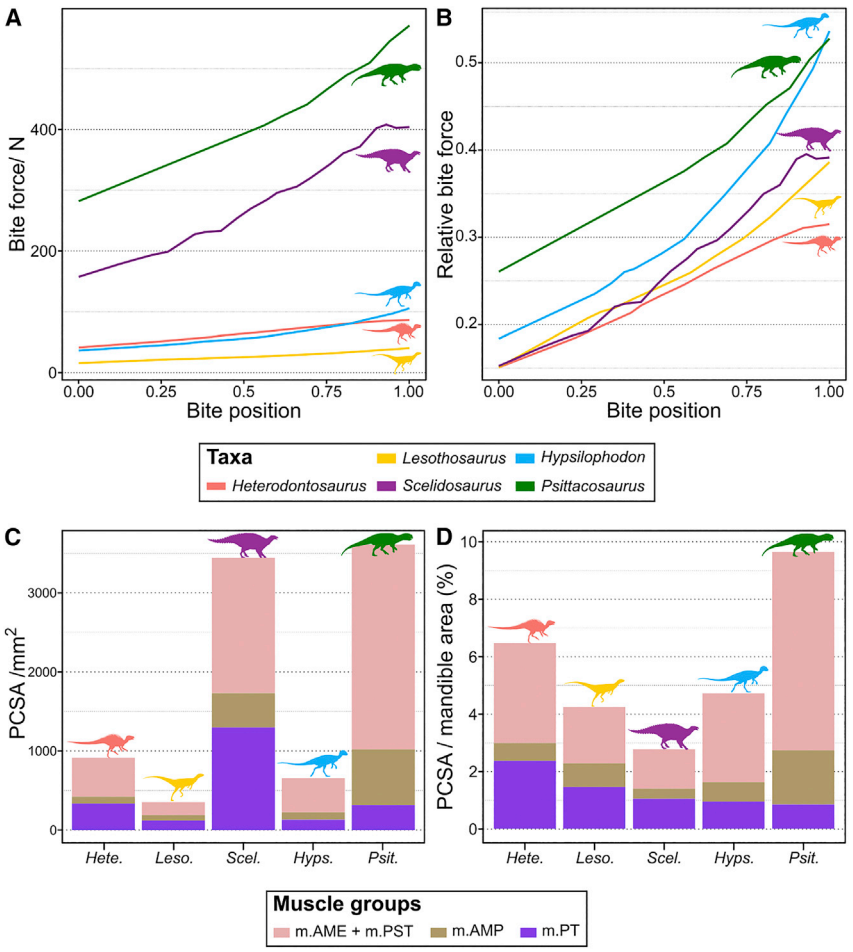

Figure 2. Calculated bite forces and muscle cross-sectional areas for ornithischian taxa

(A and B) Absolute (A) and relative (B) (calculated as input muscle force:output bite force) bite force for unilateral bites at all biting positions, as obtained from finite-element modeling of the mandible of all study taxa. Bite position is given as a proportion from 0 (biting at the anterior tip of the jaws) through to 1 (biting at the posteriormost tooth).

(C and D) Absolute (C) and size-standardized (D) (by dividing by the total surface area of the mandible) estimated physiological cross-sectional areas (PCSAs) of the jaw adductor muscles as calculated for the study taxa. Muscle PCSA is proportional to contractile force. Contributions from the temporal muscles (m. adductor mandibulae externus group and m. pseudotemporalis), the adductor mandibulae posterior, and palatal muscles (m. pterygoideus group) indicated in pink, brown, and purple, respectively.

See Tables S1 and S3 for individual muscle volumes and Tables S4 and S5 for full bite force results.

apparatus[32–37] that, in some deeply nested taxa, paralleled—or even exceeded—those of extant ungulates in complexity.[35,38–40] Although the evolution of feeding-related characters has been documented within ornithischian clades in some detail (e.g., Weishampel,[34] Ősi et al.,[36] and Tanoue et al.[41]), and repeated morphofunctional trends have been identified,[22,36,42] a previous lack of biomechanical data from early-diverging members of these lineages means that the morphofunctional pathways to herbivory have remained obscure. FEA of these five key ornithischian taxa—the omnivorous[43,44] early ornithischian *Lesothosaurus* as an exemplar of plesiomorphic ornithischian cranial morphology,[45] and early-diverging members of the major ornithischian clades that independently acquired specialized high-fiber herbivory[21] (the heterodontosaurid *Heterodontosaurus*, thyreophoran *Scelidosaurus*, ornithopod *Hypsilophodon*, and ceratopsian *Psittacosaurus*) —provides a comparative overview into the patterns of morphological change accompanying dietary specialization

Synthesis of results demonstrates that acquisitions of herbivory involved a combination of divergence and convergence in morphological evolution and functional outcomes. Increased bite force output was found among early-diverging members of Heterodontosauridae, Thyreophora, Ornithopoda, and Ceratopsia, and increased absolute mandible robustness, as measured by lower functionally induced stress magnitudes, was observed in *Heterodontosaurus*, *Scelidosaurus*, and *Psittacosaurus*. This pattern is consilient with other observed examples of convergence in morphofunctional character evolution between ornithischian clades.[21,22,42] Furthermore, the differences in functional outcomes between these taxa and *Lesothosaurus* match those observed in other herbivorous tetrapod clades relative to omnivorous outgroups[46–54] and with increased distance along the omnivory-herbivory spectrum[55,56] (although patterns may be more complicated across broader phylogenetic scales[57]). Similar trends toward increased mechanical advantage, as seen in ornithopods and ceratopsians, also occurred in herbivorous sauropodomorphs,[58] non-avian theropods,[51] squamates,[47] early mammals,[50] ungulates,[59] waterfowl,[60] and some other birds,[61] although fundamental differences in the structure of the jaw apparatus limit convergence between these taxa. Nevertheless, comparison of these results reveals common functional signals in biting efficiency associated with the independent acquisitions of herbivory in ornithischian clades, and among amniotes across broad taxonomic and size ranges. However, more detailed biomechanical comparison indicates fundamental differences underpinning the distinct modes of herbivory exhibited by these ornithischian taxa. These were achieved through larger overall adductor muscle forces in *Heterodontosaurus*, greater absolute body size in *Scelidosaurus*, increased mechanical efficiency in *Hypsilophodon*, and both increased efficiency and increased overall adductor volume in *Psittacosaurus* (Figures 1, 2, and 4). Comparison of relative reconstructed adductor muscle volumes (Figures 2C and 2D) allows these functional signals to be parsed in more detail. *Heterodontosaurus*, *Lesothosaurus*, and *Scelidosaurus* exhibit relatively large pterygoideus muscles, similar to those of sauropodomorph and theropod outgroups,[62] and subvertical external adductors

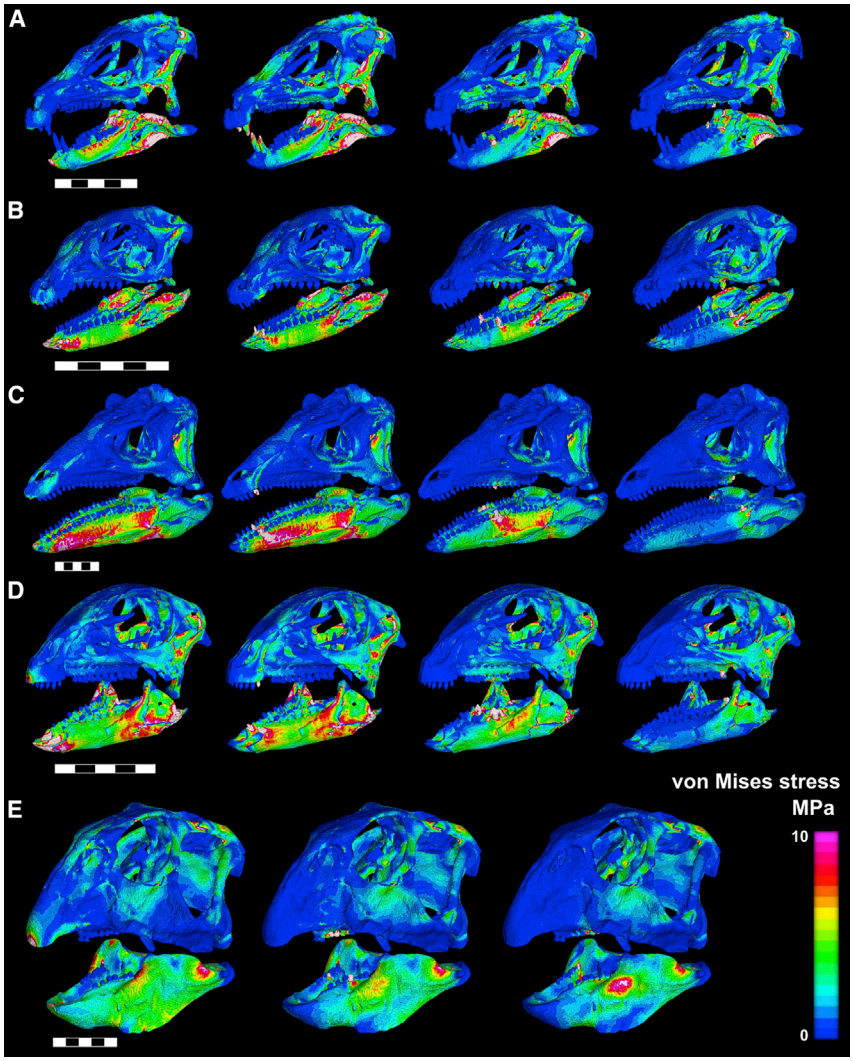

Figure 3. Results from the unscaled FEA of ornithischian taxa

von Mises stress contour plots for (A) *Heterodontosaurus*, (B) *Lesothosaurus*, (C) *Scelidosaurus*, (D) *Hypsilophodon*, and (E) *Psittacosaurus* in oblique left lateral view. Results are shown for bites at (from left) the anterior beak, the last premaxillary tooth, and opposing dentary tooth (absent for *Psittacosaurus* which lacks premaxillary teeth), the middle maxillary tooth and opposing dentary tooth, and the final tooth position. Scale bars, 50 mm.

driving orthal bites.[62] By contrast, *Hypsilophodon* and *Psittacosaurus* exhibit a more inclined adductor chamber and expansion of the more mechanically advantageous temporal muscle groups relative to the pterygoideus muscles (Figures 1, 2C, and 2D), as also seen in more later-diverging ornithischians,[62] some sauropods,[63] and some herbivorous squamates.[46]

Mapping these data onto ornithischian phylogeny (Figure 1), and considering the combination of plesiomorphic and apomorphic characters present in each taxon, enables consideration of the biomechanical significance of the patterns of character acquisition in each clade, illuminating the pathways through which the distinct feeding apparatus of each group evolved. Heterodontosaurids are defined by trophic-related characters of the dentition,[64] with Early Jurassic taxa, including *Heterodontosaurus*, exhibiting numerous craniodental features (e.g., closely packed high-crowned teeth, ventral deflection of the jaw joint, enhanced adductor musculature) that are inferred to be specializations for processing tough plant material.[64,65] Here, these are shown to be associated with a relatively robust skull and increased overall bite force (as a result of jaw adductor muscle expansion) but with relatively low biting efficiency, in contrast to other herbivorous taxa.[47,50,51,60] This difference is due, in part, to the large relative contribution of the pterygoideus musculature (Figures 2C and 2D), which inserts on the caudal end of the mandible and confers lower mechanical advantage than the temporal muscles during vertical biting. The low mechanical advantage in *Heterodontosaurus* would have compromised biting efficiency for the sake of greater jaw closing speed and a wider gape, outcomes that would be unexpected among herbivorous taxa[47,50,51] but that are consistent with the demands of prey capture during potential facultative omnivory in heterodontosaurids.[66] Although jaw adduction in *Heterodontosaurus* would have been primarily orthal,[64,67] driven by the subvertical temporal muscles,[62] the low angle of the pterygoideus muscles—although making them less efficient at delivering vertical bite forces—may have enabled them to drive possible subordinate palinal movements,[62,68] as part of a varied feeding repertoire. Consequently, the distinctive biomechanical signal of this taxon might be the result of both ecological and behavioral requirements.

Increased efficiency in *Hypsilophodon* and *Psittacosaurus* is associated with a suite of new craniodental[21,32–34,41] (e.g., taller coronoid process, asymmetric tooth enamel, caudal expansion of the toothrow, and reduction in postdentary elements) and myological[42,62] (e.g., relative expansion of temporal musculature, and greater inclination of the adductor chamber) characters that evolved in parallel between Ornithopoda and Ceratopsia, and were further elaborated independently in the more deeply nested members of both clades.[21,32–34,41,42] These attributes resulted in a functional complex that would have maximized efficiency at posterior biting positions (Figure 2B), with the powerful temporal muscles, inclined adductor chamber and shortened postdentary region resulting in an orthopalinal powerstroke,[69] as characterized previously for Late Cretaceous ornithopods and ceratopsians,[32,33,37,70] which was stabilized by the vertically oriented pterygoideus musculature.[60,71] Consequently, the evolution of this character complex in early ornithopods and

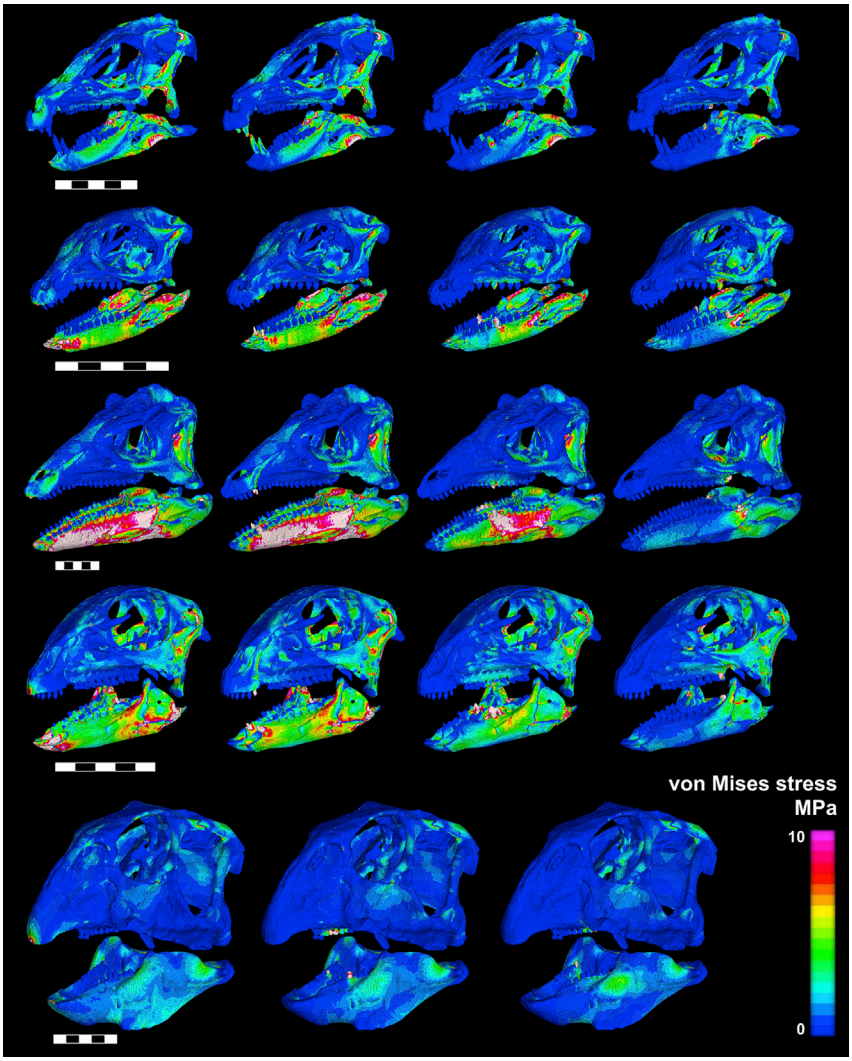

Figure 4. von Mises stress contour plots from scaled FEA of the cranium and mandible of the study ornithischian taxa

Results from models scaled to account for differences in absolute size between study taxa. Taxa, from top to bottom: *Heterodontosaurus*, *Lesothosaurus*, *Scelidosaurus*, *Hypsilophodon*, and *Psittacosaurus*. Results are for simulated bilateral bites at, from left to right; the anterior beak; the final premaxillary tooth; and opposing dentary tooth; (absent for *Psittacosaurus*, which lacks premaxillary teeth), the middle maxillary tooth and opposing dentary tooth, and the posteriormost maxillary and dentary tooth positions. Scale bars, 50 mm. See Figure S2 for additional FEA results.

ceratopsians not only permitted trituration of fibrous plant material, but also underpinned the later evolution of sophisticated oral processing in these clades.[21,22,32,34,37,41] Further, the major performance differences between *Hypsilophodon* and *Psittacosaurus* (Figures 2 and 3), due to the unique character combinations diagnosing their respective clades, appear to represent incipient states of the derived functional complexes observed in more deeply nested ornithopod and ceratopsian taxa. For example, the increased cranial robustness and expanded adductor chamber of *Psittacosaurus* result from several ceratopsian synapomorphies (rostral bone, highly flared jugals, and transversely broadened skull) that were acquired early in the history of the clade and retained in later ceratopsians (which also possessed jaw systems dominated by high bite forces).[32,33,37] Similarly, the lower bite forces and higher functionally induced stresses, but greater maximum bite efficiency, of *Hypsilophodon* is consistent with an emphasis on extensive oral processing between the cheek-teeth that has been documented in more phylogenetically nested ornithopods (e.g., Weishampel,[34] Mallon and Anderson,[37] Ostrom,[70] and Mallon and Anderson[72]).

Consequently, these results indicate that, despite their shared ancestry, distinct morphofunctional responses to the demands of high-fiber herbivory were possible in Ornithopoda and Ceratopsia and that these initial responses shaped the subsequent trajectories of morphological and ecological evolution in these clades.

By contrast, early thyreophorans exhibit few specializations of the feeding apparatus, with low relative performance across all metrics in *Scelidosaurus*, which instead exhibits increased absolute performance as a consequence of its greater overall body size. Thyreophora was the first ornithischian clade to reach large body sizes, exhibiting an evolutionary shift toward gigantism as early as the Early Jurassic, whereas large size did not occur in either Ornithopoda or Ceratopsia until much later in the Jurassic or Cretaceous.[73] The size-dependent performance of *Scelidosaurus* provides an explanation for this discrepancy: whereas other ornithischian clades responded to the challenges of obligate herbivory through morphofunctional changes to the feeding apparatus, thyreophorans instead initially responded through increased body size, both increasing the absolute performance of the feeding apparatus and permitting a longer digestive tract,[21] enabling extended gut retention time[74] as an alternative to extensive oral processing. Thyreophorans occupied a narrower total range of body sizes than neornithischians, with only one[75] potential small-bodied taxon (adult size of <100 kg) known after the Early Jurassic.[73] Although greater craniodental specialization is observed in deeply nested ankylosaur taxa,[36] thyreophorans generally exhibited lower relative bite forces than other ornithischian groups,[42] and the early assembly of a size-specific functional complex within Thyreophora, including low relative cranial performance and extensive gut fermentation,[22,74] may have constrained the clade to a subset of larger body size niches. The adoption of this different herbivorous strategy in Thyreophora may be due to multiple, non-mutually exclusive factors, such as the absence of other large-bodied ornithischians during the Early Jurassic[73] or

finer-scale differences in foraging ecology (e.g., early-onset of bulk-feeding,[73] necessitating long gut retention times[21]), although these hypotheses are difficult to test given the scarcity of direct dietary evidence from early ornithischian taxa.[76] Nevertheless, the differences in relative bite forces between *Scelidosaurus*, *Hypsilophodon*, and *Psittacosaurus* are hypothesized to represent the plesiomorphic conditions of the divergent ecologies exhibited by more deeply nested thyreophoran, ornithopod, and ceratopsian taxa during the Late Cretaceous.[37,72] The sample of early-diverging taxa examined here captures emergent differences in both the anatomy and cranial function of these taxa, which became more exaggerated in their later relatives. Consequently, despite the parallel evolution of complex craniodental systems among these clades,[21,22,32,34,36,37,42,74] each appears to have been canalized in specific regions of morphospace due to disparate functional regimes that were established early in their evolutionary histories.

Quantitative biomechanical comparisons between the feeding apparatuses of early-diverging members of the major ornithischian lineages demonstrate that each evolved a fundamentally different, independently derived solution to the challenges posed by high-fiber herbivory. For example, each of these clades diverged in characters that directly impact on the ability to use tough plant resources, such as bite efficiency[47,50–53,60] and stress accommodation.[49,77] This discovery reveals a previously unappreciated diversity among the feeding apparatuses of early ornithischian taxa, with character combinations underpinning distinct feeing modes: unspecialized morphology in the omnivorous[43,44] *Lesothosaurus*; broad performance consistent with a varied diet[43,66] in heterodontosaurids; reliance on gut-processing[74] in *Scelidosaurus*; efficient oral processing[34] in *Hypsilophodon*; and adaptations toward the exertion and accommodation for large bite forces in *Psittacosaurus*, which may have further permitted consumption of particularly hard or tough foods.[69] Furthermore, these results indicate that repeated morphofunctional trends between these lineages[22,42] were the result of "many-to-one mapping" of unique character combinations onto similar functional outcomes,[9,20,78] as opposed to repeated convergence toward specific solutions,[4–6] shared constraints,[2,9,14–16] or low trait dimensionality[79,99] limiting diversification along predictable axes. In addition, it provides an example of the cryptic functional diversity that is often masked by similarities in gross morphology,[17] highlighting the importance of quantitative biomechanical modeling in testing putative instances of evolutionary convergence, and in integrating both anatomical and functional data into palaeobiological reconstructions.

The pervasiveness of convergence has been used to argue for the primacy of adaptation in driving evolutionary patterns[13]—sufficiently powerful to make evolution predictable, as clades will repeatedly find the same solutions to similar ecological problems.[4–6] Although there are many examples of convergent evolution,[1,2,4,5,9] especially between closely related taxa,[80] whether it represents a dominant, or even relatively common, phenomenon remains unclear, as counter examples of non-convergence—taxa responding divergently to common pressures—are rarely compared or documented.[81] The recognition of divergent pathways to herbivory between ornithischian dinosaur clades provides an important example of non-convergence between related taxa through macroevolutionary time. Rather than driving convergent evolution, adaptation toward a plant-based diet instead prompted the assembly of distinct morphofunctional complexes early in ornithischian evolution. These early adaptations may have constrained the succeeding axes of variance explored by each clade due to positive feedback loops between co-varying characters[21] and the biomechanical unviability of specific character combinations,[22] leading to continued functional and ecological separation between the deeply nested members of these clades.[37,72] This example highlights that convergent evolution, even between related taxa adapting to seemingly similar ecologies, is not inevitable and, although certain aspects of evolution—such as selection for absolute bite performance—may be repeatable and predictable, the morphofunctional pathways through which these are achieved are not. Instead, the regions of morphospace explored by clades will be delimited by their idiosyncratic phylogenetic histories,[22] so that previous evolutionary events—including the acquisition of distinct ecological adaptations[1]—may prevent complete convergence between taxa. This combination of biological innovation and phylogenetic contingency means that morphofunctional evolution is not easily predictable across macroevolutionary timescales.[1,3,81]

STAR★METHODS

Detailed methods are provided in the online version of this paper and include the following:

- KEY RESOURCES TABLE
- RESOURCE AVAILABILITY
  - Lead contact
  - Materials availability
  - Data code and availability
- EXPERIMENTAL MODEL AND SUBJECT DETAILS
- METHOD DETAILS
  - Institutional abbreviations
  - CT-scanning
  - Osteological reconstruction
  - Muscle reconstruction
- QUANTIFICATION AND STATISTICAL ANALYSIS
  - Muscle force calculation
  - Finite-element model construction and boundary conditions
  - Model loading
  - Constraints and model iterations
  - Model comparison

SUPPLEMENTAL INFORMATION

Supplemental information can be found online at https://doi.org/10.1016/j.cub.2022.12.019.

ACKNOWLEDGMENTS

We thank Vincent Fernandez and Brett Clark at the Natural History Museum, London, for their help in microCT scanning the *Hypsilophodon* and *Scelidosaurus* material used in this study. Further thanks go to Ryan Ridgley (Ohio University) for assistance in microCT scanning of NHMUK PV RU B17 and to

Timothy Ryan, Avrami Grader, and Phillip M. Halek (Centre for Quantitative Imaging, Pennsylvania State University) for their help in microCT scanning of NHMUK PV RU B23, the specimens of *Lesothosaurus* used herein. Thanks also go to Chris Lamb (Royal Veterinary College) for assistance scanning the *Heterodontosaurus* specimen SAM PK K1332. We thank Sheena Kaal (formerly of the SAM) for access to material in her care. Finally, we wish to thank two anonymous reviewers whose comments improved the quality of this manuscript. This work was funded by NERC grant no. NE/R000077/1, awarded to P.M.B. and L.B.P.

AUTHOR CONTRIBUTIONS

P.M.B. and L.B.P. conceived the study. Osteological models were produced by L.B.P. (*Heterodontosaurus*, *Lesothosaurus*, and *Scelidosaurus*), M.E.H.J. (*Hypsilophodon*), S.L. (*Psittacosaurus*), and D.J.B. (*Hypsilophodon*). Muscle reconstructions were produced by D.J.B. Finite-element models were prepared by D.J.B. and L.B.P., and analyses were performed by D.J.B. D.J.B. wrote the paper with input from all other authors.

DECLARATION OF INTERESTS

The authors declare no competing interests.

INCLUSION AND DIVERSITY

We support inclusive, diverse, and equitable conduct of research.

Received: August 24, 2022
Revised: September 28, 2022
Accepted: December 8, 2022
Published: January 4, 2023

REFERENCES

1. Blount, Z.D., Lenski, R.E., and Losos, J.B. (2018). Contingency and determinism in evolution: replaying life's tape. Science *362*, eaam5979.
2. Mahler, D.L., Weber, M.G., Wagner, C.E., and Ingram, T. (2017). Pattern and process in the comparative study of convergent evolution. Am. Nat. *190*, S13–S28.
3. Gould, S.J. (1989). Wonderful Life (Norton).
4. Morris, S.C. (2010). Evolution: like any other science it is predictable. Philos. Trans. R. Soc. Lond. B Biol. Sci. *365*, 133–145.
5. McGhee, G.R. (2011). Convergent Evolution: Limited Forms Most Beautiful (The MIT Press).
6. Vermeij, G.J. (2006). Historical contingency and the purported uniqueness of evolutionary innovations. Proc. Natl. Acad. Sci. USA *103*, 1804–1809.
7. Gavrilets, S., and Losos, J.B. (2009). Adaptive radiation: contrasting theory with data. Science *323*, 732–737.
8. Nosil, P., Flaxman, S.M., Feder, J.L., and Gompert, Z. (2020). Increasing our ability to predict contemporary evolution. Nat. Commun. *11*, 5592.
9. Losos, J.B. (2011). Convergence, adaptation, and constraint. Evolution *65*, 1827–1840.
10. Mahler, D.L., Ingram, T., Revell, L.J., and Losos, J.B. (2013). Exceptional convergence on the macroevolutionary landscape in island lizard radiations. Science *341*, 292–295.
11. Moen, D.S., Morlon, H., and Wiens, J.J. (2016). Testing convergence versus history: convergence dominates phenotypic evolution for over 150 million years in frogs. Syst. Biol. *65*, 146–160.
12. Esquerré, D., and Scott Keogh, J. (2016). Parallel selective pressures drive convergent diversification of phenotypes in pythons and boas. Ecol. Lett. *19*, 800–809.
13. Maraun, M., Erdmann, G., Schulz, G., Norton, R.A., Scheu, S., and Domes, K. (2009). Multiple convergent evolution of arboreal life in oribatid mites indicates the primacy of ecology. Proc. Biol. Sci. *276*, 3219–3227.
14. Gould, S.J. (2002). The Structure of Evolutionary Theory (Harvard University Press).
15. Wake, D.B., Wake, M.H., and Specht, C.D. (2011). Homoplasy: from detecting pattern to determining process and mechanism of evolution. Science *331*, 1032–1035.
16. Bright, J.A., Marugán-Lobón, J., Cobb, S.N., and Rayfield, E.J. (2016). The shapes of bird beaks are highly controlled by nondietary factors. Proc. Natl. Acad. Sci. USA *113*, 5352–5357.
17. Lautenschlager, S., Brassey, C.A., Button, D.J., and Barrett, P.M. (2016). Decoupled form and function in disparate herbivorous dinosaur clades. Sci. Rep. *6*, 26495.
18. Losos, J.B., Jackman, T.R., Larson, A., Queiroz, K., and Rodriguez-Schettino, L. (1998). Contingency and determinism in replicated adaptive radiations of island lizards. Science *279*, 2115–2118.
19. Alfaro, M.E., Bolnick, D.I., and Wainwright, P.C. (2005). Evolutionary consequences of many-to-one mapping of jaw morphology to mechanics in labrid fishes. Am. Nat. *165*, E140–E154.
20. Wainwright, P.C. (2007). Functional versus morphological diversity in macroevolution. Annu. Rev. Ecol. Evol. Syst. *38*, 381–401.
21. Barrett, P.M. (2014). Paleobiology of herbivorous dinosaurs. Annu. Rev. Earth Planet. Sci. *42*, 207–230.
22. Button, D.J., and Zanno, L.E. (2020). Repeated evolution of divergent modes of herbivory in non-avian dinosaurs. Curr. Biol. *30*, 158–168.e4.
23. Bell, P.R., Snively, E., and Shychoski, L. (2009). A comparison of the jaw mechanics in hadrosaurid and ceratopsid dinosaurs using finite element analysis. Anat. Rec. (Hoboken) *292*, 1338–1351.
24. Maiorino, L., Farke, A.A., Kotsakis, T., Raia, P., and Piras, P. (2018). Who is the most stressed? Morphological disparity and mechanical behavior of the feeding apparatus of ceratopsian dinosaurs (Ornithischia, Marginocephalia). Cretaceous Research *84*, 483–500.
25. Taylor, A.C., Lautenschlager, S., Qi, Z., and Rayfield, E.J. (2017). Biomechanical evaluation of different musculoskeletal arrangements in *Psittacosaurus* and implications for cranial function. Anat. Rec. (Hoboken) *300*, 49–61.
26. Lautenschlager, S. (2017). From bone to pixel-fossil restoration and reconstruction with digital techniques. Geol. Today *33*, 155–159.
27. Holliday, C.M. (2009). New insights into dinosaur jaw muscle anatomy. Anat. Rec. (Hoboken) *292*, 1246–1265.
28. Biewener, A.A. (1989). Scaling body support in mammals: limb posture and muscle mechanics. Science *245*, 45–48.
29. Dumont, E.R., Grosse, I.R., and Slater, G.J. (2009). Requirements for comparing the performance of finite element models of biological structures. J. Theor. Biol. *256*, 96–103.
30. Ross, C.F., and Metzger, K.A. (2004). Bone strain gradients and optimization in vertebrate skulls. Ann. Anat. *186*, 387–396.
31. King, G. (1996). Reptiles and Herbivory (Chapman & Hall).
32. Ostrom, J.H. (1964). A functional analysis of jaw mechanics in the dinosaur *Triceratops*. Postilla Yale Peabody Museum Nat. Hist. *88*, 1–35.
33. Ostrom, J.H. (1966). Functional morphology and evolution of the ceratopsian dinosaurs. Evolution *20*, 290–308.
34. Weishampel, D.B. (1984). Evolution of jaw mechanisms in ornithopod dinosaurs. Adv. Anat. Embryol. Cell Biol. *87*, 1–109.
35. Bramble, K., Leblanc, A.R.H., Lamoureux, D.O., Wosik, M., and Currie, P.J. (2017). Histological evidence for a dynamic dental battery in hadrosaurid dinosaurs. Sci. Rep. *7*, 15787.
36. Ősi, A., Prondvai, E., Mallon, J., and Bodor, E.R. (2017). Diversity and convergences in the evolution of feeding adaptations in ankylosaurs (Dinosauria: Ornithischia). Hist. Biol. *29*, 539–570.
37. Mallon, J.C., and Anderson, J.S. (2015). Jaw mechanics and evolutionary paleoecology of the megaherbivorous dinosaurs from the Dinosaur Park Formation (Upper Campanian) of Alberta, Canada. J. Vertebr. Paleontol. *35*, e904323.

38. Erickson, G.M., Krick, B.A., Hamilton, M., Bourne, G.R., Norell, M.A., Lilleodden, E., and Sawyer, W.G. (2012). Complex dental structure and wear biomechanics in hadrosaurid dinosaurs. Science *338*, 98–101.

39. Erickson, G.M., Sidebottom, M.A., Kay, D.I., Turner, K.T., Ip, N., Norell, M.A., Sawyer, W.G., and Krick, B.A. (2015). Wear biomechanics in the slicing dentition of the giant horned dinosaur *Triceratops*. Sci. Adv. *1*, e1500055.

40. LeBlanc, A.R.H., Reisz, R.R., Evans, D.C., and Bailleul, A.M. (2016). Ontogeny reveals function and evolution of the hadrosaurid dinosaur dental battery. BMC Evol. Biol. *16*, 152.

41. Tanoue, K., Grandstaff, B.S., You, H.L., and Dodson, P. (2009). Jaw mechanics in basal Ceratopsia (Ornithischia, Dinosauria). Anat. Rec. (Hoboken) *292*, 1352–1369.

42. Nabavizadeh, A. (2016). Evolutionary trends in the jaw adductor mechanics of ornithischian dinosaurs. Anat. Rec. (Hoboken) *299*, 271–294.

43. Barrett, P.M. (2000). Prosauropod dinosaurs and iguanas: speculations on the diets of extinct reptiles. In Evolution of Herbivory in Terrestrial Vertebrates, H.-D. Sues, ed. (Cambridge University Press), pp. 42–78.

44. Sciscio, L., Knoll, F., Bordy, E.M., de Kock, M.O., and Redelstorff, R. (2017). Digital reconstruction of the mandible of an adult *Lesothosaurus diagnosticus* with insight into the tooth replacement process and diet. PeerJ *5*, e3054.

45. Norman, D.B., Witmer, L.M., and Weishampel, D.B. (2004). Basal Ornithischia. In The Dinosauria, Second Edition, D.B. Weishampel, P. Dodson, and H. Osmolska, eds. (University of California Press), pp. 325–334.

46. Herrel, A., Aerts, P., and De Vree, F. (1998). Ecomorphology of the lizard feeding apparatus: A modelling approach. Neth. J. Zool. *48*, 1–25.

47. Stayton, C.T. (2006). Testing hypotheses of convergence with multivariate data: morphological and functional convergence among herbivorous lizards. Evolution *60*, 824–841.

48. Christiansen, P., and Wroe, S. (2007). Bite forces and evolutionary adaptations to feeding ecology in carnivores. Ecology *88*, 347–358.

49. Tseng, Z.J., and Flynn, J.J. (2018). Structure-function covariation with nonfeeding ecological variables influences evolution of feeding specialization in Carnivora. Sci. Adv. *4*, eaao5441.

50. Morales-Garciá, N.M., Gill, P.G., Janis, C.M., and Rayfield, E.J. (2021). Jaw shape and mechanical advantage are indicative of diet in Mesozoic mammals. Commun. Biol. *4*, 242.

51. Ma, W., Pittman, M., Butler, R.J., and Lautenschlager, S. (2021). Macroevolutionary trends in theropod dinosaur feeding mechanics. Curr. Biol. *32*, 677–686.e3.

52. Sacco, T., and Van Valkenburgh, B. (2004). Ecomorphological indicators of feeding behaviour in the bears (Carnivora: Ursidae). J. Zool. *263*, 41–54.

53. Samuels, J.X. (2009). Cranial morphology and dietary habits of rodents. Zool. J. Linn. Soc. *156*, 864–888.

54. Dumont, E.R., Dávalos, L.M., Goldberg, A., Santana, S.E., Rex, K., and Voigt, C.C. (2012). Morphological innovation, diversification and invasion of a new adaptive zone. Proc. Biol. Sci. *279*, 1797–1805.

55. Herrel, A., Vanhooydonck, B., and Van Damme, R. (2004). Omnivory in lacertid lizards: adaptive evolution or constraint? J. Evol. Biol. *17*, 974–984.

56. Herrel, A., Huyghe, K., Vanhooydonck, B., Backeljau, T., Breugelmans, K., Grbac, I., Van Damme, R., and Irschick, D.J. (2008). Rapid large-scale evolutionary divergence in morphology and performance associated with exploitation of a different dietary resource. Proc. Natl. Acad. Sci. USA *105*, 4792–4795.

57. Isip, J.E., Jones, M.E.H., and Cooper, N. (2022). Clade-wide variation in bite-force performance is determined primarily by size, not ecology. Proc. Biol. Sci. *289*, 20212493.

58. Button, D.J., Barrett, P.M., and Rayfield, E.J. (2017). Craniodental functional evolution in sauropodomorph dinosaurs. Paleobiology *43*, 435–462.

59. Janis, C.M. (1995). Correlations between craniodental morphology and feeding behavior in ungulates: reciprocal illumination between living and fossil taxa. In Functional Morpohlogy in Vertebrate Paleontology, J.J. Thomason, ed. (Cambridge University Press), pp. 76–98.

60. Olsen, A.M. (2017). Feeding ecology is the primary driver of beak shape diversification in waterfowl. Funct. Ecol. *31*, 1985–1995.

61. Navalón, G., Bright, J.A., Marugán-Lobón, J., and Rayfield, E.J. (2019). The evolutionary relationship among beak shape, mechanical advantage, and feeding ecology in modern birds. Evolution *73*, 422–435.

62. Nabavizadeh, A. (2020). Cranial musculature in herbivorous dinosaurs: a survey of reconstructed anatomical diversity and feeding mechanisms. Anat. Rec. (Hoboken) *303*, 1104–1145.

63. Button, D.J., Rayfield, E.J., and Barrett, P.M. (2014). Cranial biomechanics underpins high sauropod diversity in resource-poor environments. Proc. Biol. Sci. *281*, 20142114.

64. Sereno, P.C. (2012). Taxonomy, morphology, masticatory function and phylogeny of heterodontosaurid dinosaurs. ZooKeys, 1–225.

65. Crompton, A.W., and Attridge, J. (1986). Masticatory apparatus of the larger herbivores during the Late Triassic and Early Jurassic times. In The Beginning of the Age of Dinosaurs, K. Padian, ed. (Cambridge University Press), pp. 223–236.

66. Butler, R.J., Porro, L.B., Galton, P.M., and Chiappe, L.M. (2012). Anatomy and cranial functional morphology of the small-bodied dinosaur *Fruitadens haagarorum* from the Upper Jurassic of the USA. PLoS One *7*, e31556.

67. Norman, D.B., Crompton, A.W., Butler, R.J., Porro, L.B., and Charig, A.J. (2011). The Lower Jurassic ornithischian dinosaur *Heterodontosaurus tucki* Crompton & Charig, 1962: cranial anatomy, functional morphology, taxonomy, and relationships. Zool. J. Linn. Soc. *163*, 182–276.

68. Thulborn, R.A. (1974). A new heterodontosaurid dinosaur (Reptilia: Ornithischia) from the Upper Triassic Red Beds of Lesotho. Zool. J. Linn. Soc. *55*, 151–175.

69. Sereno, P.C., Xijin, Z., and Lin, T. (2010). A new psittacosaur from Inner Mongolia and the parrot-like structure and function of the psittacosaur skull. Proc. Biol. Sci. *277*, 199–209.

70. Ostrom, J.H. (1961). Cranial morphology of the hadrosaurian dinosaurs of North America. Bull. Am. Museum Nat. Hist. *122*, 33–186.

71. Lull, R.S. (1908). The cranial musculature and the origin of the frill in ceratopsian dinosaurs. Am. J. Sci. *25*, 387–399.

72. Mallon, J.C., and Anderson, J.S. (2014). The functional and palaeoecological implications of tooth morphology and wear for the megaherbivorous dinosaurs from the Dinosaur Park Formation (Upper Campanian) of Alberta, Canada. PLoS One *9*, e98605.

73. Benson, R.B.J., Campione, N.E., Carrano, M.T., Mannion, P.D., Sullivan, C., Upchurch, P., and Evans, D.C. (2014). Rates of dinosaur body mass evolution indicate 170 million years of sustained ecological innovation on the avian stem lineage. PLoS Biol. *12*, e1001853.

74. Weishampel, D.B., and Jianu, C.-M. (2000). Plant-eaters and ghost lineage: dinosaurian herbivory revisited. In Evolution of Herbivory in Terrestrial Vertebrates: Perspectives from the Fossil Record, H.-D. Sues, ed. (Cambridge University Press), pp. 123–143.

75. Riguetti, F.J., Apesteguía, S., and Pereda-Suberbiola, X. (2022). A new Cretaceous thyreophoran from Patagonia supports a South American lineage of armoured dinosaurs. Sci. Rep. *12*, 11621.

76. Salgado, L., Canudo, J.I., Garrido, A.C., Moreno-Azanza, M., Martínez, L.C.A., Coria, R.A., and Gasca, J.M. (2017). A new primitive neornithischian dinosaur from the Jurassic of Patagonia with gut contents. Sci. Rep. *7*, 42778.

77. Mitchell, D.R., Sherratt, E., Ledogar, J.A., and Wroe, S. (2018). The biomechanics of foraging determines face length among kangaroos and their relatives. Proc. Biol. Sci. *285*, 20180845.

78. Alfaro, M.E., Bolnick, D.I., and Wainwright, P.C. (2004). Evolutionary dynamics of complex biomechanical systems: an example using the four-bar mechanism. Evolution *58*, 495–503.

79. Stayton, C.T. (2008). Is convergence surprising? An examination of the frequency of convergence in simulated datasets. J. Theor. Biol. *252*, 1–14.

80. Ord, T.J., and Summers, T.C. (2015). Repeated evolution and the impact of evolutionary history on adaptation. BMC Evol. Biol. *15*, 137.

81. Losos, J.B. (2010). Adaptive radiation, ecological opportunity, and evolutionary determinism. American Society of Naturalists E. O. Wilson award address. Am. Nat. *175*, 623–639.

82. Butler, R.J., Upchurch, P., and Norman, D.B. (2008). The phylogeny of the ornithischian dinosaurs. J. Syst. Palaeontol. *6*, 1–40.

83. Tanoue, K., You, H., and Dodson, P. (2009). Comparative anatomy of selected basal ceratopsian dentitions. Can. J. Earth Sci. *46*, 425–439.

84. Porro, L.B., Witmer, L.M., and Barrett, P.M. (2015). Digital preparation and osteology of the skull of *Lesothosaurus diagnosticus* (Ornithischia: Dinosauria). PeerJ *3*, e1494.

85. Norman, D.B. (2021). *Scelidosaurus harrisonii* (Dinosauria: Ornithischia) from the Early Jurassic of Dorset, England: biology and phylogenetic relationships. Zool. J. Linn. Soc. *191*, 1–86.

86. Galton, P.M. (1974). The ornithischian dinosaur *Hypsilophodon* from the Wealden of the Isle of Wight. Bull. Br. Museum Nat. Hist. Geol. *25*, 1–152.

87. Witmer, L.M. (1995). The extant phylogenetic bracket and the importance of reconstructing soft tissues in fossils. In Functional Morphology in Vertebrate Paleontology, J. Thomason, ed. (Cambridge University Press), pp. 19–33.

88. Holliday, C.M., Tsai, H.P., Skiljan, R.J., George, I.D., and Pathan, S. (2013). A 3D interactive model and atlas of the jaw musculature of *Alligator mississippiensis*. PLoS One *8*, e62806.

89. Jones, M.E.H., Button, D.J., Barrett, P.M., and Porro, L.B. (2019). Digital dissection of the head of the rock dove (*Columba livia*) using contrast-enhanced computed tomography. Zoological Lett. *5*, 17.

90. Jones, M.E.H., Curtis, N., O'Higgins, P., Fagan, M., and Evans, S.E. (2009). The head and neck muscles associated with feeding in *Sphenodon* (Reptilia: Lepidosauria: Rhynchocephalia). Palaeontol. Electron. *12*, 7A.

91. Haas, G. (1955). The jaw musculature in *Protoceratops* and in other ceratopsians. Am. Museum Novit. 1–24.

92. Witmer, L.M. (1997). The evolution of the antorbital cavity of archosaurs: a study in soft-tissue reconstruction in the fossil record with an analysis of the function of pneumaticity. J. Vertebr. Paleontol. *17*, 1–76.

93. Sereno, P.C. (1991). *Lesothosaurus*, "Fabrosaurids," and the early evolution of Ornithischia. J. Vertebr. Paleontol. *11*, 168–197.

94. Thomason, J.J. (1991). Cranial strength in relation to estimated biting forces in some mammals. Can. J. Zool. *69*, 2326–2333.

95. Cost, I.N., Middleton, K.M., Sellers, K.C., Echols, M.S., Witmer, L.M., Davis, J.L., and Holliday, C.M. (2020). palatal biomechanics and its significance for cranial kinesis in *Tyrannosaurus rex*. Anat. Rec. (Hoboken) *303*, 999–1017.

96. Lautenschlager, S. (2013). Cranial myology and bite force performance of *Erlikosaurus andrewsi*: a novel approach for digital muscle reconstructions. J. Anat. *222*, 260–272.

97. Lautenschlager, S., Witmer, L.M., Altangerel, P., and Rayfield, E.J. (2013). Edentulism, beaks, and biomechanical innovations in the evolution of theropod dinosaurs. Proc. Natl. Acad. Sci. USA *110*, 20657–20662.

98. Bates, K.T., and Falkingham, P.L. (2012). Estimating maximum bite performance in *Tyrannosaurus rex* using multi-body dynamics. Biol. Lett. *8*, 660–664.

99. Bright, J.A., and Gröning, F. (2011). Strain accommodation in the zygomatic arch of the pig: a validation study using digital speckle pattern interferometry and finite element analysis. J. Morphol. *272*, 1388–1398.

100. Bright, J.A. (2012). The importance of craniofacial sutures in biomechanical finite element models of the domestic pig. PLoS One *7*, e31769.

101. Zapata, U., Metzger, K., Wang, Q., Elsey, R.M., Ross, C.F., and Dechow, P.C. (2010). Material properties of mandibular cortical bone in the American alligator, *Alligator mississippiensis*. Bone *46*, 860–867.

102. Porro, L.B., Holliday, C.M., Anapol, F., Ontiveros, L.C., Ontiveros, L.T., and Ross, C.F. (2011). Free body analysis, beam mechanics, and finite element modeling of the mandible of *Alligator mississippiensis*. J. Morphol. *272*, 910–937.

103. Sellers, K.C., Schmiegelow, A.B., and Holliday, C.M. (2019). The significance of enamel thickness in the teeth of *Alligator mississippiensis* and its diversity among crocodyliforms. J. Zool. *309*, 172–181.

104. Button, D.J., Barrett, P.M., and Rayfield, E.J. (2016). Comparative cranial myology and biomechanics of *Plateosaurus* and *Camarasaurus* and evolution of the sauropod feeding apparatus. Palaeontology *59*, 887–913.

105. Metzger, K.A., Daniel, W.J.T., and Ross, C.F. (2005). Comparison of beam theory and finite-element analysis with in vivo bone strain data from the alligator cranium. Anat. Rec. A Discov. Mol. Cell. Evol. Biol. *283*, 331–348.

106. Reed, D.A., Porro, L.B., Iriarte-Diaz, J., Lemberg, J.B., Holliday, C.M., Anapol, F., and Ross, C.F. (2011). The impact of bone and suture material properties on mandibular function in *Alligator mississippiensis*: testing theoretical phenotypes with finite element analysis. J. Anat. *218*, 59–74.

107. Bright, J.A. (2014). A review of paleontological finite element models and their validity. J. Paleontol. *88*, 760–769.

108. Bright, J.A., and Rayfield, E.J. (2011). Sensitivity and ex vivo validation of finite element models of the domestic pig cranium. J. Anat. *219*, 456–471.

109. Grosse, I.R., Dumont, E.R., Coletta, C., and Tolleson, A. (2007). Techniques for modeling muscle-induced forces in finite element models of skeletal structures. Anat. Rec. (Hoboken) *290*, 1069–1088.

110. Davis, J.L., Santana, S.E., Dumont, E.R., and Grosse, I.R. (2010). Predicting bite force in mammals: 2D vs. 3D lever models. J. Exp. Biol. *213*, 1844–1851.

111. Rayfield, E.J. (2007). Finite element analysis and understanding the biomechanics and evolution of living and fossil organisms. Annu. Rev. Earth Planet. Sci. *35*, 541–576.

STAR★METHODS

KEY RESOURCES TABLE

REAGENT or RESOURCE	SOURCE	IDENTIFIER
Deposited data		
Ornithischian CT-scan data	This paper	Morphosource: Project 000486311 (https://www.morphosource.org/projects/000486311?)
Software and algorithms		
Avizo (v. 2020.1)	ThermoFisher Scientific	https://www.thermofisher.com
Strand7 (R3.1.1)	Strand7	https://www.strand7.com/
MatLab	MathWorks	https://www.mathworks.com/products/matlab.html
BoneLoad	Grosse et al.[109] and Davis et al.[110]	http://faculty.usi.edu/jldavis2/research/
Other		
Ornithischian skull models	This paper	figshare: https://doi.org/10.6084/m9.figshare.21750494
Psittacosaurus skull osteological model	Taylo et al.[25]	https://anatomypubs.onlinelibrary.wiley.com/doi/10.1002/ar.23489

RESOURCE AVAILABILITY

Lead contact

Further information and requests for resources and reagents should be directed to and will be fulfilled by the Lead Contact, D.J. Button (david.button@bristol.ac.uk).

Materials availability

This study did not generate new unique reagents. The CT scan data collected for this study are available at Morphosource: Project 000486311 (https://www.morphosource.org/projects/000486311?) and the skull models generated and analyzed in this study are available at figshare: https://doi.org/10.6084/m9.figshare.21750494.

Data code and availability

The CT scan data collected for this study are available at Morphosource: Project 000486311 (https://www.morphosource.org/projects/000486311?) and the skull models generated and analyzed in this study are available at figshare: https://doi.org/10.6084/m9.figshare.21750494.

EXPERIMENTAL MODEL AND SUBJECT DETAILS

The CT-scan data analyzed in this study was collected from fossil specimens housed in public trust repositories (full specimen and CT-scan details are given in Data S1). No data from privately held specimens was included in this study.

METHOD DETAILS

Institutional abbreviations

AM = Albany Museum, Grahamstown, South Africa; AMNH = American Museum of Natural History, New York, USA; BRSMG = Bristol City Museum, UK; NHMUK = Natural History Museum, London, UK; NM = National Museum, Bloemfontein, South Africa; SAM = Iziko South African Museum, Cape Town, South Africa.

CT-scanning

Specimens of *Scelidosaurus harrisonii* and *Hypsilophodon foxii* were each subject to X-ray micro-Computed Tomography (XμCT) using a Nikon XTH ST 225 CT-scanner (Nikon metrology, Leuven, Belgium) at the Natural History Museum, London. Details of the scan parameters used for each specimen are given in Data S1. For each, the 'minimize ring artefacts' approach was used, implying an acquisition in step-by-step mode (i.e. rotation motor stopped during radiograph acquisition). Tomographic reconstruction was done using CT agent software (Nikon metrology) based on the filtered-back projection algorithm. Prior to the reconstruction, a beam hardening correction was applied, using the automated approach of CT agent, manually defining material and background

with a threshold. CT data were exported as 16-bit raw data, selecting the 32-bit range by excluding 0.2% of values on both sides of the histogram. The parameters of the CT scans of *Lesothosaurus* material used to produce the osteological model are described in Porro et al.,[84] and those of *Psittacosaurus* in Taylor et al.[25]

Osteological reconstruction

The osteological models for each taxon were produced in Avizo (v. 2020.1, ThermoFisher Scientific), employing retrodeformation procedures into order to reconstruct original morphology through filling cracks and holes, restoring missing elements, and correcting warpage.[26] These procedures are described in more detail per each taxon below.

Heterodontosaurus tucki

The model of *Heterodontosaurus tucki* used herein is based upon CT scans of SAM PK K1332, with additional information from visual comparison to other *Heterodontosaurus* specimens (SAM PK K10487, AM 4766, NM QR 1788 and AMNH 24000). To produce a symmetrical, 3D model of the skull, the best preserved of each paired element was first selected. For the cranium, the majority of elements were taken from the better-preserved left side of the skull, with the exception of the palpebral, which was taken from the right side of the skull. For the midline elements, the (fused) vomers and basioccipital were used as preserved. However, the right sides of both the supraoccipital and basisphenoid are deformed: consequently, the left half of these elements were segmented and mirrored to produce a symmetrical reconstruction of the bone. Holes and cracks in skeletal elements were patched, and the broken dorsal and ventral parts of the quadrate shaft realigned. In addition, the upper temporal bar has suffered plastic deformation on both sides of SAM PK K1332. To correct this deformation, a series of landmarks, defining a smooth curve from the back of the main body of the postorbital to the front of the main body of the squamosal were created, and the bones were warped to fit this curve. Finally, because the posteriormost tooth of the cranium was missing, the tooth immediately anterior to it was duplicated and moved to occupy the empty tooth space. Once these digital repairs were completed, all elements were duplicated and rearticulated with their antimeres to produce a symmetrical reconstruction of the cranium.

The mandible was reconstructed wholly on the basis of the better-preserved left hemimandible, with the exception of the midline predentary, which is preserved attached to the right hemimandible. Cracks and small holes in these elements were repaired, including closure of much of the gap between the upper and lower tracts of the surangular of SAM PK K1332 to more closely resemble the condition preserved in other *Heterodontosaurus* specimens. The left hemimandible was then mirrored to produce a complete mandible.

Lesothosaurus diagnosticus

The *Lesothosaurus* osteological model used herein is a composite based upon NHMUK PV RU B17 and NHMUK PV RU B23. The best-preserved of each paired element between these two specimens was selected. Specifically, the fused vomers, basisphenoid, basioccipital and predentary were taken from NHMUK PV RU B17, as were the left main body of the premaxilla, posterior third of the jugal, prootic, laterosphenoid, surangular, angular, prearticular and articular, and the right palatine, ectopterygoid, pterygoid, dentary and splenial. The supraoccipital and fused parietals, the left posterior process of the premaxilla, maxilla, lacrimal, palpebral, anterior two-thirds of the jugal, quadrate, exoccipital, and the right nasal, prefrontal, frontal, postorbital, squamosal and quadrate were taken from NHMUK PV RU B23. The small quadratojugal had to be almost completely reconstructed because it was so incomplete in the available scanned specimens; this reconstruction was done using images of, and information from, NHMUK PV R8501.

The internarial bar and the walls of the opisthotic between the exoccipital and the prootic and laterosphenoid were reconstructed through interpolation, constrained by contacts with surrounding bones. Only a single well-preserved tooth is present in the maxilla of NMHUK PV RU B17: this tooth was copied and used to restore the other maxillary teeth. The dentary of NHMUK PV RU B17 is preserved in two blocks: the separate pieces were re-joined. The dentary teeth were then restored based upon the isolated and displaced teeth in these blocks, with the first three after a small, presumably anterior tooth, and the others from a larger, more typical dentary tooth.

The restored cranial elements were then combined and mirrored as necessary to rearticulate a right half of the cranium and mandible. These were each then mirrored and recombined to produce a complete model of the skull.

Scelidosaurus harrisonii

The *Scelidosaurus* model used herein is a composite of NHMUK PV R1111 and BRSMG Ce12785. Specifically, the basioccipital, basisphenoid, fused vomers, both laterosphenoids, exoccipitals and opisthotics, the left pterygoid, and the right squamosal, quadrate, nasal, prefrontal, frontal, prefrontal, frontal, postfrontal, parietal, ectopterygoid, posterior dentary, splenial, coronoid, surangular, angular, prearticular and articular were taken from NMHUK PV R1111. The right premaxilla, maxilla, lacrimal, jugal, postorbital and associated ossification, quadratojugal, palatine and anterior dentary were then taken from BRSMG Ce12785.

For the cranium, the right premaxilla of BRSMG Ce12785 is preserved in two pieces, which were repositioned and merged with each other. The anterior part of the nasal and the internarial bar were restored using interpolation. The missing fourth maxillary tooth was replaced by duplicating the third maxillary tooth and moving it to occupy this socket. The missing supraorbital element was restored following.[85] For the mandible, the anterior and posterior ends of the dentary, preserved in NHMUK PV R1111 and BRSMG Ce12785 respectively, were merged, with gaps in the toothrow replaced through replicating the second dentary tooth of BRSMG Ce12785. Finally, a small predentary capping the anterior ends of the dentaries was recreated, based upon the dimensions of these elements and the predentaries of other thyreophoran taxa. The restored elements were then mirrored as necessary and rearticulated to yield the osteological model used here.

Hypsilophodon foxii

The model of *Hypsilophodon foxii* used herein is based primarily upon the holotype, NHMUK PV R197. However, this specimen is incomplete, lacking the predentary and anterior end of the dentary, much of the articular, and the palpebral, and has suffered extensive taphonomic deformation and fragmentation of the skull roof. As a result, missing or excessively damaged elements were based upon more complete or less deformed examples from NHMUK PV R196, NHMUK PV R2470, and NHMUK PV R2477. Specifically, the left main body of the premaxilla, maxilla, lacrimal, jugal, quadratojugal, bottom of the quadrate wing, pterygoid, ectopterygoid, palatine, vomer, posterior dentary, surangular, coronoid, splenial, angular, prearticular and anterior part of the articular, and the right ascending process of the premaxilla and squamosal were taken from NHMUK PV R197. The braincase, the left nasal, frontal, postorbital, parietal, and main body of the quadrate, and the right prefrontal were taken from NHMUK PV R2477. The anterior end of the left dentary, up to the second tooth, was taken from NHMUK PV R196, and the predentary from NHMUK PV R2470.

Comparison of measurements from overlapping elements/partial elements indicates that those of NHMUK PV R2477 are consistently ~12-20% larger than those of NHMUK PV R197, similar to the difference between postcranial measurements from these specimens,[86] suggesting size variance between the two was approximately isometric. Elements from NHMUK PV R2477 were hence scaled based upon their preserved dimensions in NHMUK PV R197. However, as NHMUK PV R197 entirely lacks the predentary, that of NHMUK PV R2470 was scaled based upon the articular facet for the predentary preserved in NHMUK PV R196. A complete articular is lacking from this material, and so the posterior end of the articular of NHMUK PV R197 was completed using that of *Lesothosaurus*. The missing palpebral was also based upon that of *Lesothosaurus*, scaled according to its corresponding articular facet in NHMUK PV R197. The palpebral is not thought to play any role in accommodating feeding-related stresses, and indeed was not resolved to do so in the analyses conducted herein. Furthermore, only the posterior end of the articular, posterior to the glenoid for the quadrate, was restored after *Lesothosaurus* and, although this restoration may affect the shape of the insertion site for the m. depressor mandibulae, this muscle was not included in the FEA performed herein. Consequently, these compromises are not believed to adversely affect the results.

Cracks and holes in these elements were repaired. The fragments of the ascending process of the right premaxilla of NHMUK PV R197 were rotated back and merged with each other, mirrored, and combined with the left premaxilla to form a complete element. The ascending process of the maxilla of NHMUK PV R197 is complete but fragmented: these fragments were pieced back together to complete the element. The angle of the anterior ramus of the pterygoid of this specimen has been warped, and the vomers are crushed and fragmented. These elements were segmented along their length and these fragments were moved back into their original positions, constrained by the positions of other bones (see below). The left nasal of NHMUK PV R2477 was straightened and positioned based upon preserved fragments of the nasal of NHMUK PV R196. The tip of the descending process of the postorbital of NHMUK PV R2477 was restored using interpolation based on the facet for this process on the surface of the jugal of NMHUK PV R197. The fragmented posterolateral wing of the left parietal of NMHUK PV R2477 was restored by rotating these pieces back together. The quadrate was mostly from NHMUK PV R2477, but with the ventral part of the quadrate wing restored using the better-preserved part of this element from NHMUK PV R197. The anterior part of the dentary of NHMUK PV R196 was merged with the rest of the dentary of NHMUK PV R197 by rotating and scaling it so that the alveolus for the second tooth of both elements matched.

These repaired elements were then mirrored to produce their antimeres and rearticulated. To ensure symmetry, the braincase and predentary were also bisected down the midline, mirrored, and these halves were stitched together. The better-preserved and constrained regions of the skull (skull roof, braincase, snout) were re-articulated first, and then used to help establish the more poorly constrained topology of the palate, in particular the vomers and the angle of the anterior ramus of the pterygoid (see above). The hemimandibles were rearticulated last, based on the morphology of the predentary and the shape of the upper toothrow.

Psittacosaurus lujiatunensis

See Taylor et al.[25] for details of the *Psittacosaurus* osteological model used herein.

Muscle reconstruction

Muscle insertion and origination sites were reconstructed on the basis of observed osteological correlates,[27] with inferences constrained based upon extant phylogenetically bracketing[87] taxa, including *Alligator*[88] and *Columba*,[89] as well as previous reconstructions of ornithischian jaw musculature.[25,42,63,65,68,70,71,85,89] A parrot-like pseudomasseter, as reconstructed in *Psittacosaurus* by Sereno et al.,[69] and m. adductor mandibulae externus ventralis, as has been suggested in *Heterodontosaurus*[64] and *Psittacosaurus*,[69] were not reconstructed due to the lack of phylogenetic, and limited osteological, evidence for these tissues,[25] and to standardize comparisons between taxa. The origination and insertion sites of the other taxa are described below and illustrated in Figure S1.

M. adductor mandibulae externus superficialis *(m.AMES)*

The m.AMES is inferred to originate from the smooth medial and medioventral surfaces of the upper temporal bar, as in lepidosaurs[27,70,86,90] and typical for non-avian dinosaurs,[27,62,70] in a level I inference.[87] Anteromedially, the extent of the m.AMES was delimited based upon a slight separation between the excavation for the m.AMES and that of the m.PSTs within the supratemporal fossa in *Heterodontosaurus*, *Lesothosaurus*, *Hypsilophodon* and *Psittacosaurus*. In *Scelidosaurus* this separation is more obvious, with distinct, deep excavations in the posterior surfaces of the postorbital medial process and the frontal reconstructed as occupied by the m.AMES and m.PSTs, respectively (Figure S1C). The m.AMES of *Lesothosaurus*, *Scelidosaurus* and *Psittacosaurus* is hence reconstructed as occupying a significant portion of the anterior part of the supratemporal fenestra, originating from most of the

posterior surface of the medial process of the postorbital. By contrast, the anteromedial extent of the m.AMES in both *Heterodontosaurus* and *Hypsilophodon* appears to have been more restricted, on the basis of both these osteological correlates and topological constraints provided by the cranium and other adductor muscles.

Posteriorly, the origin of the m.AMES extends onto the anterior face of the medial process of the squamosal, and is separated from the insertion area for the m.AMEM by a slight ridge in *Heterodontosaurus*, *Lesothosaurus*, *Scelidosaurus* and *Psittacosaurus*. In *Lesothosaurus*, the origin for the m.AMES also appears to extend slightly into a well-defined sulcus on the ventrolateral surface of the anterolateral process of the squamosal[84] (Figure S1B). *Scelidosaurus* exhibits a smooth ventrolateral surface on the squamosal anteromedial process, which is bounded dorsally by its overhanging lateral surface,[85] and continuous with the scar for the m.AMES on its ventromedial surface. The origination site for the m.AMES in *Scelidosaurus* was hence inferred to extend onto the ventrolateral surface of the squamosal, similar to the reconstruction of Norman,[85] although extending less far anteriorly and posteriorly (Figure S1C). An attachment of the m.AMES onto the ventrolateral surface of the squamosal was also suggested in *Hypsilophodon* by Galton,[86] but was rejected here due to topological constraints and the absence of an osteological correlate in this region.

In *Heterodontosaurus*, a large excavation is present on the lateral surface of the supratemporal bar and ventral process of the postorbital, bounded dorsally by a longitudinal ridge, itself continuous anteriorly with a pronounced ridge on the postorbital, and posteriorly with the squamosal rim. This area was considered to represent an additional insertion area for the m.AMES the on lateral surface of the supratemporal bar similar to, but extending less far posteriorly than, the 'm.AMESX' of Norman et al.[67] (Figure S1A, see also similar reconstructions by Nabavizadeh,[42] Sereno,[64] and Crompton and Attridge[65]). Nonetheless, the novel nature of this correlate makes this origin a level III inference.

The m.AMES is reconstructed as inserting onto the dorsolateral edge of the surangular in all five taxa (Figure S1), as is typical for ornithischians,[25,27,62,64,65,70,85,86,91] and sauropsids in general,[27,90] in a level I inference. In *Lesothosaurus* this insertion site is marked by the smooth, ventrolaterally beveled dorsal margin of the surangular, which is bounded ventrally by a slight ridge. In *Scelidosaurus*, *Hypsilophodon* and *Psittacosaurus* it is marked by a more vertically oriented fossa in the surangular, which extends onto the lateral surface of the coronoid process in *Hypsilophodon*. In *Scelidosaurus* this fossa is bound ventrally by a strong lateral shelf, reminiscent of the condition observed in theropods[27] (Figure S1C). *Heterodontosaurus* possesses an unusual surangular morphology, where its dorsal edge is composed of two bony tracts, delineated by a groove.[64,67] Norman et al.[67] reconstructed the m.AMES as inserting ventral to these struts, onto the thickened surface of the angular, resulting in this muscle passing lateral to the lower temporal bar. This arrangement is problematic, however, as this it would be unique among archosaurs.[64] Instead, the m.AMES is here reconstructed as inserting onto the dorsal and lateral surfaces of the upper tract, and extending onto the dorsal surface of the lower tract, (Figure S1A, cf. Sereno[64]), based on the smooth surfaces of these areas and the unambiguous insertion of the m.AMES onto the dorsolateral surface of the surangular, as in other ornithischian taxa.[27,64]

M. adductor mandibulae externus medialis *(m.AMEM)*

The m.AMEM is reconstructed as originating from the posterior region of the supratemporal fossa as is typical for non-avian dinosaurs (e.g., Taylor et al.,[25] Holliday,[27] Nabavizadeh,[62] and Ostrom[70]), occupying the anterior surface of the medial process of the squamosal, part of the lateral surface of the parietal, and the dorsolateral surface of the opisthotic (Figure S1), in a level I inference. The lateral distinction between this insertion site and that of the m.AMES is demarcated by a ridge in *Heterodontosaurus*, *Lesothosaurus*, *Scelidosaurus* and *Psittacosaurus*. In *Hypsilophodon*, the m.AMEM is reconstructed as filling the entirety of a circular fossa on the anterior face of the squamosal, distinct from the shallower scar for the m.AMES. The medial distinction between this insertion site and that of the m.AMEP is difficult to ascertain,[27] but is based upon a slight change in curvature and difference in shape of the parietal within the supratemporal fossa: this fossa is more prominent in *Scelidosaurus* and *Hypsilophodon*. The ventral margin of this insertion is not distinct but is considered to be coincident with a swelling of the braincase, based upon topological constraints within the reconstructed adductor chamber.

The m.AMEM is reconstructed as inserting onto the dorsomedial surface of the surangular, as in previous reconstructions of ornithischian taxa[25,27,62,67,70,86] and typical for sauropsids.[27,70,90] However, the generally ambiguous nature of this muscle in extant taxa can make it difficult to separate from the m.AMES and m.AMEP,[5] making this inference a level I' inference.[27] Here, the m.AMEM was reconstructed inserting onto the surangular posterior to the coronoid eminence of each taxon, leaving a narrow scar slightly separated from the more anterior insertion reconstructed for the m.AMEP (see below). Norman[85] reconstructed the m.AMEM of *Scelidosaurus* as attaching to the coronoid eminence via a bodenaponeurosis. However, this arrangement was not adopted here, due to the presence of a clear osteological correlate for the m.AMEM on the surangular (Figure S1C).

M. adductor mandibulae externus profundus *(m.AMEP)*

The m.AMEP is reconstructed as originating from the medial wall of the supratemporal fossa, occupying the lateral surfaces of the middle portion of the parietal and the laterosphenoid, in all five taxa, as is typical for dinosaurs,[27] including ornithischians.[27,62,64,67,86] This inference is a level I inference for all five ornithischian taxa. Dorsally, this origination site extends onto a low sagittal crest in *Heterodontosaurus*, *Scelidosaurus*, *Hypsilophodon* and *Psittacosaurus* (Figures S1A and S1C–S1E) whereas the supratemporal fossa is lower in *Lesothosaurus* (Figure S1B). The boundary between the origins for the m.AMEP and the m.PSTs is marked by a vertical, anterodorsally oriented, ridge on the parietal in *Heterodontosaurus*, *Lesothosaurus* and *Scelidosaurus* as also seen in some other non-avian dinosaurs,[27] and by a more subtle change in curvature of the parietal surface in *Hypsilophodon*[27] and *Psittacosaurus*. Topological constraints between the reconstructed volumes of the m.AMEP and m.PSTs also help to delimit their relative extents in these taxa.

The m.AMEP is reconstructed as inserting into the coronoid region of the mandible, as is typical for ornithischians[25,27,42,62,64,69,70,85] and sauropsids in general.[27,70,90] In all five taxa, a distinct, circular scar is present on the dorsomedial surface of the apex of the

coronoid process, wrapping around onto its dorsal and, slightly, its dorsolateral surfaces (Figure S1). The m.AMEP is reconstructed as inserting only onto the coronoid process in *Heterodontosaurus*, *Lesothosaurus* and *Hypsilophodon*. In *Scelidosaurus* and *Psittacosaurus* it spreads onto the anterior edge of the dorsomedial surface of the surangular, delimited posteriorly by what appears to be a slight separation between this insertion correlate and the scar for the m.AMEM. This reconstructed insertion site is hence a level I inference for all five taxa.

M. pseudotemporalis superficialis *(m.PSTs)*

The m.PSTs was reconstructed as originating from the anteromedial portion of the supratemporal fossa of all five taxa, as observed in lepidosaurs[27] and previously reconstructed in ornithischians[25,62,67,70,85,86] in a Level I inference.[27] There is a slight separation between the scars for the m.PSTs and the m.AMES (see above): whereas the m.PSTs spread anterolaterally onto the posteromedial corner of the postorbital in *Lesothosaurus* (Figure S1B) and *Hypsilophodon* (Figure S1D) it was instead confined to the frontal in *Heterodontosaurus*, *Scelidosaurus* and *Psittacosaurus* (Figures S1A, S1C, and S1E). Posteriorly, the m.PSTs originated from the lateral surface of the anterior half of the parietal, bounded posteriorly by the origin of the m.AMEP (see above).

The insertion site for the m.PSTs is variable in extant sauropsids, as it inserts onto the medial aspect of the coronoid region in lepidosaurs and most extant birds, but into the medial mandibular fossa in crocodilians and the majority of ratites.[27] Here, the m.PSTs was reconstructed as inserting into the anterior portion of the elongate mandibular fossa in *Heterodontosaurus*, *Lesothosaurus*, *Scelidosaurus* and *Psittacosaurus*, after,[25,27] in a Level I inference. This reconstruction contrasts with previous reconstructions of *Heterodontosaurus*[67] and *Scelidosaurus*,[85] which included the m.PSTs inserting onto the coronoid process. This arrangement was rejected here, however, due both to the relatively elongate mandibular fossa in these taxa, which is more similar to outgroups possessing an insertion of this muscle into the adductor fossa,[27] and spatial constraints, with this alternative path for the m.PSTs being precluded by the m.AMEP. By contrast, the m.PSTs was inferred to insert into a slightly depressed region on the medial surface of the coronoid in *Hypsilophodon* (Figure S1D), similar to its previously reconstructed position in both *Hypsilophodon*[86] and more derived ornithopods.[27,62,70] This region was further reconstructed to accommodate the m.PSTs, rather than the m.AMEP, due to spatial constraints resulting from alternative configurations of these muscles. Nonetheless, the variability of this insertion in extant sauropsids, and the potentially ambiguous nature of this osteological correlate, make this a Level II' inference.

The m. pseudotemporalis profundus (m.PSTp) is reconstructed as originating from the surface of the epipterygoid in dinosaurs.[27] However, an ossified epipterygoid is absent in many ornithischians, which may have lost this muscle.[27] Consequently, no attempt was made to reconstruct the m.PSTp. Although an ossified epipterygoid is present in *Scelidosaurus*[85] the m.PSTp was not reconstructed for this taxon as: 1) it is unlikely to have made a significant contribution to jaw adduction[85]; and 2) this permits equivalent comparisons between it and other ornithischians that lack this element.

M. adductor mandibulae posterior *(m.AMP)*

The m.AMP was reconstructed as originating from the anterolateral surface of the quadrate in all five taxa, as-in other sauropsids[27] and previous reconstructions of this muscle in these taxa.[25,27,62,64,67,69,70,86] This insertion is marked by a deep excavation in the anterior surface of the quadrate shaft in *Heterodontosaurus*[67] (Figure S1A), but only by a shallow concavity or flattening of the surface in other taxa. The m.AMP is reconstructed as inserting into the adductor fossa of the mandible in all five taxa, as in previous reconstructions of ornithischians[25,27,62,69,70,86] and sauropsids generally.[27,90] The highly conserved nature of these origination and insertion sites within Sauropsida[27] make these attachments a level I inference for all taxa.

M. pterygoideus dorsalis *(m.PTd)*

The m.PTd originates on the dorsal surfaces of the bones at the posterior end of the palate in sauropsids.[27] Consequently, it was reconstructed as originating from the dorsal surfaces of the pterygoid, ectopterygoid and palatine in all five taxa, as in previous reconstructions of ornithischian adductor musculature,[25,62,64,69,70,85,86] in a level I inference. The anterior extent of this origination area can be difficult to discern[27] but may be marked in dinosaurs by a fossa on the dorsal surface of the palatines, posterior to an anterior pneumatic fossa.[92] The fossa on the dorsal surfaces of the palatines is continuous with a depression in the pterygoid and ectopterygoid and bound laterally by a sharp ridge, as observed in *Lesothosaurus*[84,93] (Figure S1B) and *Hypsilophodon* (Figure S1D). The anterior extent of the m.PTd insertion in *Scelidosaurus* was taken as consistent with an arced, smooth dorsal surface of the palatine, and that of *Psittacosaurus* is marked by a depression in the dorsal surface of the pterygoid flange. The extent of the m.PTd is less clear in *Heterodontosaurus*, but is constrained anteriorly by the robust prefrontal-lacrimal pillar.[67] It is here reconstructed as originating from the depressed dorsal surfaces of the pterygoid flange and posterior palatine, and a second depression in the dorsal surfaces of the ecopterygoid and the posterior end of the maxillary shelf (Figure S1A), similar to the reconstruction of Norman et al.[67]

The m.PTd inserts onto the medial surfaces of the prearticular and articular in sauropsids,[27] leading to the attachment that has been universally reconstructed in ornithischians (e.g., Taylor et al.,[25] Holliday,[27] Nabavizadeh,[42] Nabavizadeh,[62] Norman,[67] Ostrom,[70] Norman,[85] Galton,[86] and Haas[91]) as a type I inference.[27] A depressed, triangular region is observed on the medial surface of the prearticular in all five ornithischian taxa. This surface, which is roughened in *Heterodontosaurus* but smooth in *Lesothosaurus*, *Scelidosaurus*, *Hypsilophodon*, and *Psittacosaurus*, was taken as the extent of the insertion site of the m.PTd (Figure S1). A distinct shelf is observed at the contact between the prearticular and angular in all five ornithischian taxa, making it unlikely that this insertion site spread onto the medial surface of the angular.

M. pterygoideus ventralis *(m.PTv)*

The m.PTv originates from the posterodorsal edge of the pterygoid in extant crocodilians and birds,[27] and so is reconstructed as having done so in ornithischians.[27,62,70,85,86,91] Specifically, the m.PTv is reconstructed here as originating from the thickened posteromedial margin of the pterygoid flange, and the smooth, thickened or concave ventral surface of the pterygoid immediately posterior

to it, in all taxa, as a level I inference. In *Lesothosaurus* and *Heterodontosaurus*, this origination site appears to have extended posteriorly to ventrally underlie the basal articulation. The m.PTv was further reconstructed as occupying an excavated pocket in this region in *Heterodontosaurus* following,[67] and as also reconstructed in some hadrosaurs.[70] By contrast, the basal articulation is well separated from the pterygoid flange in *Scelidosaurus*, *Hypsilophodon* and *Psittacosaurus*, making such an extent less likely.

In dinosaurs, the m.PTv is typically reconstructed as wrapping around the ventral margin of the mandible to insert onto the ventral and lateral surfaces of the angular, and the lateral surface of the surangular, as-in extant crocodilians and some birds.[27] In *Hypsilophodon* and *Psittacosaurus*, this insertion is marked by a smooth region on the ventrolateral surface of the mandible and the retroarticular process, ventral to the jaw joint[25,86] (Figures S1D and S1E). In *Heterodontosaurus* and *Lesothosaurus* this insertion site is far more extensive and bounded dorsally by a ridge on the surangular (Figures S1A and S1B), similar to the condition observed in many theropods.[27] A deep excavation in the lateral surface of the retroarticular process of *Heterodontosaurus* further evidences the insertion of a substantial m.PTv in this region.[67] In *Heterodontosaurus*, the anterior extent of the insertion of the m.PTv is bounded by a strong dorsal curvature of the ventral margin of the mandible[67] (Figure S1A). The anterior extent of this insertion area is less well-defined in *Lesothosaurus*, but is here taken as consistent with the anteriormost extent of the ridge on the surangular, resulting in the insertion of the m.PTv terminating just posterior to the posteroventral extent of the splenial (Figure S1B). As in the other ornithischian taxa, *Scelidosaurus* bears a prominent scar for the m.PTv along the ventrolateral surface of the mandible.[85] In addition, it is also reconstructed as attaching along an anteriorly extending depression on the lateral surface of the mandible, continuous with this scar and bounded dorsally by a strong ridge on the surangular (Figure S1C), similar to the condition observed in *Heterodontosaurus* and *Lesothosaurus*. The presence of clear osteological correlates make the insertion of the m.PTv a type I inference for all five taxa.

QUANTIFICATION AND STATISTICAL ANALYSIS

Muscle force calculation

Adductor muscle contractile forces for *Heterodontosaurus*, *Lesothosaurus*, *Scelidosaurus* and *Hypsilophodon* were estimated via the 'dry skull method.'[94] First, the total volume of each muscle was measured using the 'measure surface area volume' module, and its length using the '3D measurement' option in the 'measurement' module. The volume of each muscle was then divided by its fiber length, estimated as equaling two-thirds of its total length following.[95] In the absence of pennation angle data from non-avian dinosaurs, a pennation angle of 0 was assumed, resulting in maximum PCSA estimates for each muscle. Contractile forces for each muscle were then calculated by multiplying PCSA estimates by a specific tension of 0.3 mm^{-2} after,[94] as in many other studies on extinct dinosaurs (e.g., Lautenschlager,[96] Lautenschlager et al.,[97] and Bates and Falkingham[98]). Reconstructed muscle volumes, lengths and maximum contractile forces are given in Table S1.

For *Psittacosaurus*, the muscle volumes calculated by Taylor et al.[25] were used herein, although the hypothetical pseudomasseter and 'adductor mandibulae externus ventralis'[69] were excluded following[25] (see above). However, as that study employed total muscle length as an estimate of fiber length, as opposed to the two-thirds value employed here following,[95] using the forces calculated by Taylor et al.[25] would systematically underestimate bite forces and induced stresses and strains in *Psittacosaurus* relative to other taxa. Consequently, these muscle forces were recalculated employing a two-thirds total length estimate of fiber length, so that results could be directly compared with other taxa in the sample ('adjusted forces' in Table S1).

Finite-element model construction and boundary conditions

The completed models were each subjected to standard mesh quality checks using the surface editor in Avizo, repairing intersecting and poor-quality elements. Following these, for each model, each cranial element and suture was imported individually into Strand7 (R3.1.1) for meshing. Here, standard checks for element quality were repeated, with violating elements repaired through a combination of manual editing and automated mesh cleaning functions. Once cleaned, this 2D surface mesh was used to produce a 3D solid mesh of linear tetrahedral bricks using the 'automesh' function within Strand7. Summary statistics of each meshed model are provided in Table S2.

Each model was composed of three separate materials: bones, teeth, and cranial sutures, modelled as a band of more compliant bricks between bones. Although necessarily simplified, modelling sutures in this way has been demonstrated to yield accurate biomechanical information.[99] Throughout model construction, cranial sutures were made at least three elements in thickness wherever possible without sacrificing morphological accuracy, in order to avoid artefacts at suture-bone boundaries.[99,100] These materials were assigned the properties of *Alligator* mandibular bone (E = 20.49 GPa, ν = 0.4[101]), and those for dentine (E = 21 GPa, ν = 0.31) and sutural tissues (E = 0.09 GPa, ν = 0.3) previously used in models of *Alligator*,[102] respectively. Enamel was not modelled due to the relative thinness of enamel in dinosaurs relative to other taxa,[103] as in previous analyses of extant archosaurs.[102] Materials were assumed to be homogenous and isotropic, as is typical in studies of extinct dinosaurs (e.g., Lautenschlager et al.,[17] Taylor et al.,[25] Button et al.,[63] Lautenschlager,[96] Lautenschlager et al.,[97] and Button et al.[104]), due to the lack of data on material anisotropy in fossil taxa. Although this simplification may compromise the accuracy of absolute stress and strain magnitudes,[102,105,106] validation studies have indicated that meaningful patterns of relative stress and strain distribution, which are our primary interest here, can still be retrieved when using isotropic material properties (e.g., Metzger et al.,[105] Bright,[107] and Bright and Rayfield[108]).

Model loading

Each model was loaded with adductor forces using BoneLoad.[109,110] This permitted the total force for each muscle to be distributed evenly across origination and insertion sites, which were mapped in Avizo as surfaces of a single voxel thickness. The total force magnitude of each muscle was then divided equally across a series of plates mapping this attachment site in Strand7, in-turn acting upon the underlying bricks. Muscle vectors were projected towards a centroid representing the reconstructed opposing insertion/origination site of the muscle: BoneLoad modifies the direction of these vectors so that they wrap around the surfaces of intervening bones, rather than travelling through them.

Two alternative load cases were then applied to each model. The first applied the muscle forces as given in Table S1, to provide a best-estimate of the 'in-vivo' bite forces and absolute performance of each taxon. The second 'scaled' comparison scaled adductor forces so that the ratio of applied force/surface area for each element in each taxon equaled that of *Lesothosaurus* (Table S3). Keeping this ratio constant between taxa standardizes for size in comparisons of von Mises stress.[29] Consequently, comparison of the relative performance of these scaled models (as measured by induced stress magnitudes) reflects differences due to variance in cranial shape and muscle orientation, rather than size, among these taxa.[29] In lieu of any information on muscle activation patterns in extinct dinosaurs, maximal loads (either absolute or scaled) for all modeled muscles were applied during each load case (equivalent to simultaneously maximal activation of all adductor muscles). Although, in life, activation patterns would have likely varied between taxa, this approach was chosen to standardize comparisons as far as possible. Varying patterns of muscle activation may alter regions of high stresses at the mandibular insertion sites in *Heterodontosaurus* and *Hypsilophodon* (Figures 3 and 4) but would not be expected to significantly affect the high bending stresses in the dentary of *Scelidosaurus* during rostrally-situated bites (Figures 3C and 4C).

Constraints and model iterations

Linear static solutions were performed for the cranium and mandible of each taxon, employing both of these alternative muscle load cases, for simulated bilateral and unilateral bites at every tooth position. All models were constrained against translation and rotation in all three principal axes at three nodes on either the quadrate condyle or articular glenoid, for cranium and mandible models, respectively. Then, for unilateral bites, a single node on each biting tooth was constrained against translation and rotation in the y-axis. For bilateral bites, a single node was constrained on each biting tooth. Bite forces were calculated for mandible models as the y-component of the reaction force of the biting tooth for unilateral bites (Table S4) or the summed forces for both teeth for bilateral bites (Table S5).

In addition to bites between each tooth position along the toothrow, models were also solved for bites at the margins of the snout and predentary bone of the lower jaw, which formed a cropping beak in ornithischians.[65] For unilateral bites at the beak, a single node was constrained on the left side of the apex of the predentary for mandible models, and the premaxilla (or rostral in *Psittacosaurus*) for cranial models. For bilateral bites at the beak, two nodes were constrained, on the left and right sides of the midline of these elements. These models were used to calculate bite forces at the predentary beak for all taxa in the same way as for the teeth (Tables S4 and S5).

Model comparison

Performance between models was compared between taxa at each biting position through comparisons of predicted bite forces, and magnitudes and distributions of functionally-induced von Mises stress. Von Mises stress represents a measure of 'overall' stress, with higher magnitudes approximating closer proximity to failure, and so a mechanically weaker structure under the current loading regime.[29,111]

Current Biology, Volume *33*

Supplemental Information

Multiple pathways to herbivory underpinned deep divergences in ornithischian evolution

David J. Button, Laura B. Porro, Stephan Lautenschlager, Marc E.H. Jones, and Paul M. Barrett

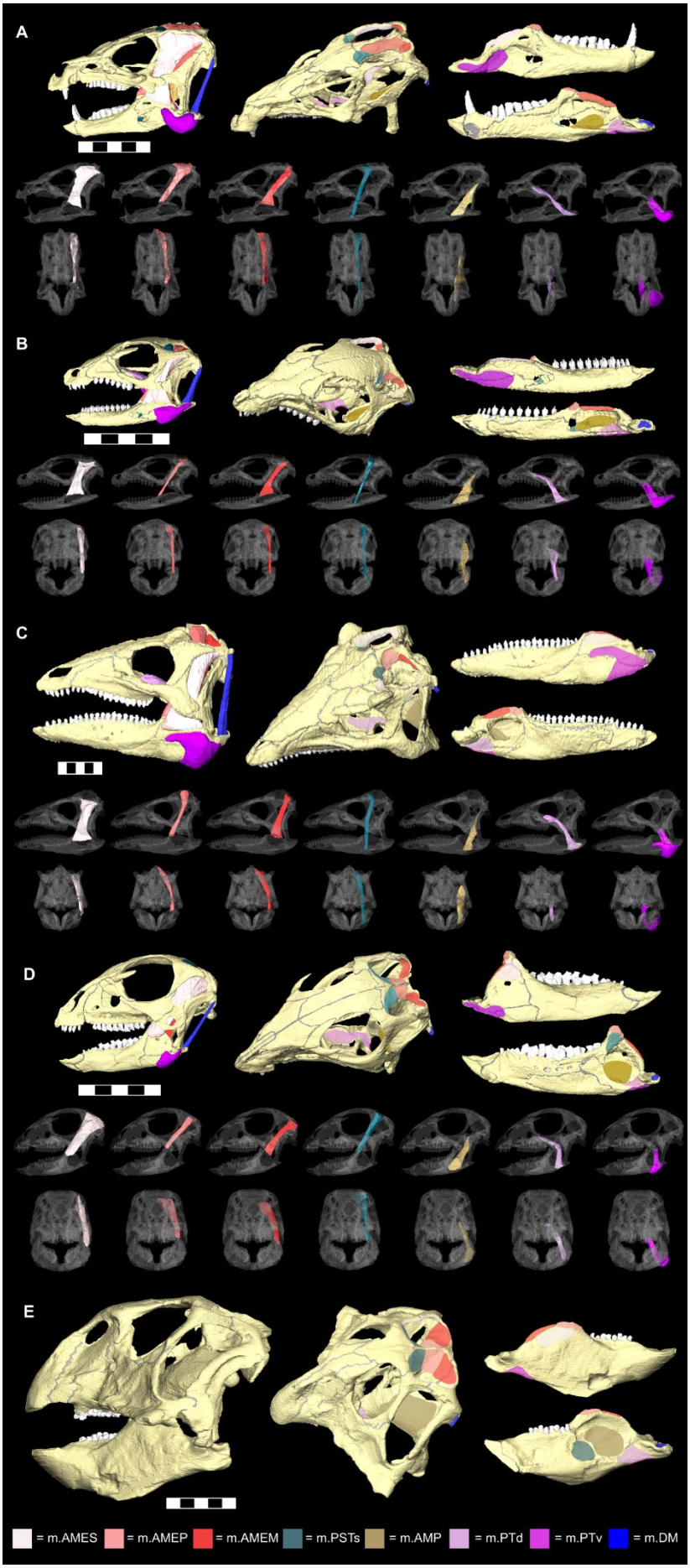
A
B
C
D
E
= m.AMES
= m.AMEP
= m.AMEM
= m.PSTs
= m.AMP
= m.PTd
= m.PTv
= m.DM

Figure S1: Reconstructed jaw muscles and attachment sites for ornithischian taxa. Related to Figure 1, and STAR Methods. A) *Heterodontosaurus*, B) *Lesothosaurus*, C) *Scelidosaurus*, D) *Hypsilophodon*, E) *Psittacosaurus*. For each taxon, complete muscle volumes are depicted on the top left, origination sites on the cranium on the top middle, and insertion sites on the mandible in lateral (above) and medial (below) views on the top right. Individual muscle volumes are then depicted in left lateral (above) and anterior (below) views, with the skull set as translucent, at the bottom. Scale bars for complete skulls with muscle = 50 mm, others not drawn to scale.

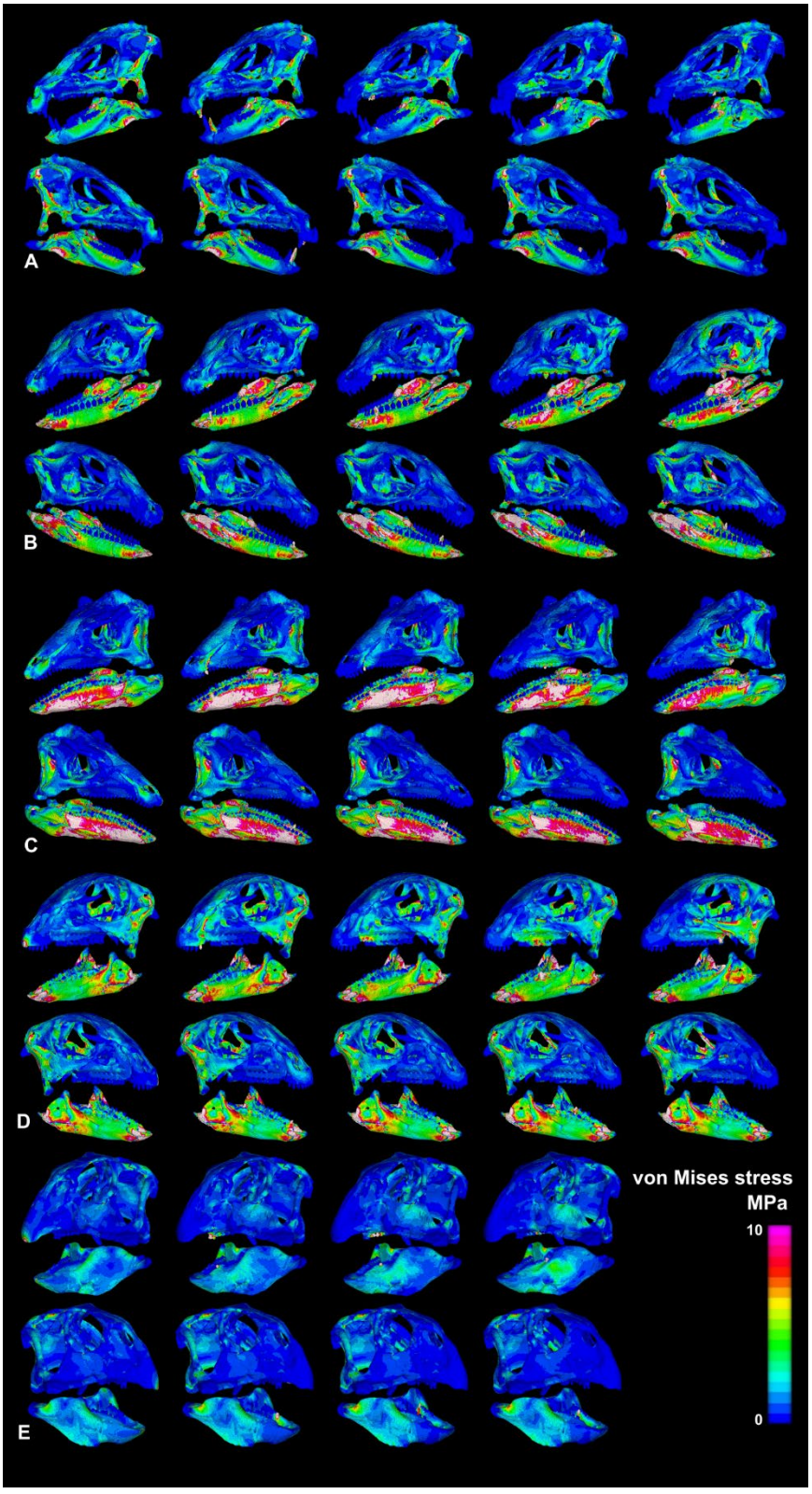
A
B
C
D
E
von Mises stress
MPa
10
0

Figure S2: von Mises stress contour plots from scaled finite-element models of ornithischian taxa, solved for unilateral bites. Related to Figure 4. Results for A) *Heterodontosaurus*, B) *Lesothosaurus*, C) *Scelidosaurus*, D) *Hypsilophodon* and E) *Psittacosaurus* for unilateral bites at (from left to right) the anterior beak, the final premaxillary tooth and opposing dentary tooth, the anteriormost maxillary tooth and opposing dentary tooth, the middle maxillary tooth and opposing dentary tooth, and the final tooth position. For each taxon, oblique lateral views of the working-side are shown on top, and the balancing side on-bottom. Skulls not drawn to scale.

Taxon	Muscle	Muscle volumes/mm3	Muscle length/mm	Fibre length/mm	PCSA	Contractile Force
Heterodontosaurus	m.AMES	3196.600	47.240	31.493	101.501	**30.450**
	m.AMEP	2674.200	59.610	39.740	67.292	**20.188**
	m.AMEM	1714.000	55.130	36.753	46.635	**13.991**
	m.PSTs	1331.600	67.140	44.760	29.750	**8.925**
	m.AMP	1113.900	38.180	25.453	43.762	**13.129**
	m.PTd	1058.300	62.560	41.707	25.375	**7.612**
	m.PTv	3295.800	34.870	23.247	141.775	**42.533**
	TOTAL	14384.400	364.730	243.153	456.091	**136.827**
Lesothosaurus	m.AMES	925.300	32.000	21.333	43.373	**13.012**
	m.AMEP	289.600	39.110	26.073	11.107	**3.332**
	m.AMEM	408.000	37.570	25.047	16.290	**4.887**
	m.PSTs	323.900	45.000	30.000	10.797	**3.239**
	m.AMP	683.100	30.000	20.000	34.155	**10.247**
	m.PTd	570.800	42.340	28.227	20.222	**6.067**
	m.PTv	803.800	30.010	20.007	40.177	**12.053**
	TOTAL	4004.500	256.030	170.687	176.120	**52.836**
Scelidosaurus	m.AMES	24173.000	97.370	64.913	372.389	**111.717**
	m.AMEP	11901.000	111.150	74.100	160.607	**48.182**
	m.AMEM	13596.000	103.010	68.673	197.981	**59.394**
	m.PSTs	11111.000	134.590	89.727	123.832	**37.149**
	m.AMP	10544.000	73.000	48.667	216.658	**64.997**
	m.PTd	12605.000	105.850	70.567	178.625	**53.588**
	m.PTv	24487.000	78.100	52.067	470.301	**141.090**
	Total	108417.000	703.070	468.713	1720.392	**516.118**
Hypsilophodon	m.AMES	2289.600	45.480	30.320	75.515	**22.654**
	m.AMEP	1270.700	42.500	28.333	44.848	**13.454**
	m.AMEM	1577.100	43.670	29.113	54.171	**16.251**
	m.PSTs	1211.000	44.300	29.533	41.005	**12.301**
	m.AMP	1097.400	34.830	23.220	47.261	**14.178**
	m.PTd	888.800	52.540	35.027	25.375	**7.612**

	m.PTv	860.200	32.060	21.373	40.246	**12.074**
	Total	9194.800	295.380	196.920	328.421	**98.526**
Psittacosaurus	**Muscle**		**Forces (Taylor et al.[25])**			**Adjusted forces**
	m.AMES		88.800			**133.200**
	m.AMEP		60.100			**90.150**
	m.AMEM		43.200			**64.800**
	m.PSTs		66.500			**99.750**
	m.AMP		70.400			**105.600**
	m.PTd		11.600			**17.400**
	m.PTv		20.100			**30.150**
	Total		360.700			**541.050**

Table S1: Reconstructed volumes and calculated contractile forces for the adductor musculature of ornithischian taxa. Related to Figure 2 and STAR Methods. Each value refers to a single muscle: the total force was hence then applied to both sides of the model. Fiber lengths were estimated as two-thirds total muscle length, following[76]. Contractile forces were calculated using a specific tension value of specific tension of 0.3 mm^{-2}, following[75]. For *Psittacosaurus*, muscle forces reconstructed by Taylor et al.[25] were adjusted to match the fiber-length assumptions made in this study: these forces were then used for FEA.

	Bricks	Plates	Nodes	Volume /mm3
Heterodontosaurus				
Cranium	1575200	20301	344441	27366.5
Mandible	2198264	33846	447129	10642.5
Lesothosaurus				
Cranium	2632367	24029	545938	12120.7
Mandible	1015544	13029	212191	3825.41
Scelidosaurus				
Cranium	2749539	24161	561522	347420
Mandible	2530998	28527	507454	171273
Hypsilophodon				
Cranium	2275729	22809	492427	22025.4
Mandible	996900	13090	204426	9437.9
Psittacosaurus				
Cranium	3150329	52332	671308	257375
Mandible	1165402	24562	255589	93639.6

Table S2: Summary of the models used in this study. Related to STAR Methods.

Taxon	Muscles	Forces	Scaled forces (cranium)	Scaled forces (mandible)
Heterodontosaurus	m.AMES	30.450	19.691	20.005
	m.AMEP	20.188	13.054	13.263
	m.AMEM	13.991	9.047	9.191
	m.PSTs	8.925	5.771	5.863
	m.AMP	13.129	8.490	8.625
	m.PTd	7.612	4.923	5.001
	m.PTv	42.533	27.504	27.943
	TOTAL	**136.827**	**88.479**	**89.892**
Cranium SA = 34465.3	Force/Cranium SA	3.970E-03	2.567E-03	NA
Mandible SA = 14092.4	Force/Mandible SA	9.709E-03	NA	6.379E-03
Lesothosaurus	m.AMES	13.012	13.012	13.012
	m.AMEP	3.332	3.332	3.332
	m.AMEM	4.887	4.887	4.887
	m.PSTs	3.239	3.239	3.239
	m.AMP	10.247	10.247	10.247
	m.PTd	6.067	6.067	6.067
	m.PTv	12.053	12.053	12.053
	TOTAL	**52.836**	**52.836**	**52.836**
Cranium SA = 20581.3	Force/Cranium SA	2.567E-03	2.567E-03	NA
Mandible SA = 8283.1	Force/Mandible SA	6.379E-03	NA	6.379E-03
Scelidosaurus	m.AMES	111.717	144.414	171.120
	m.AMEP	48.182	62.284	73.802
	m.AMEM	59.394	76.778	90.976
	m.PSTs	37.149	48.022	56.903
	m.AMP	64.997	84.021	99.559
	m.PTd	53.588	69.272	82.082
	m.PTv	141.090	182.384	216.113
	TOTAL	**516.118**	**667.175**	**790.555**
Cranium SA = 259885	Force/Cranium SA	1.986E-03	2.567E-03	NA
Mandible SA = 123935	Force/Mandible SA	4.164E-03	NA	6.379E-03

Hypsilophodon	m.AMES	22.654	20.793	20.360
	m.AMEP	13.454	12.349	12.092
	m.AMEM	16.251	14.916	14.605
	m.PSTs	12.301	11.290	11.055
	m.AMP	14.178	13.013	12.742
	m.PTd	7.612	6.987	6.841
	m.PTv	12.074	11.082	10.851
	TOTAL	**98.526**	**90.429**	**88.547**
Cranium SA = 35224.8	Force/Cranium SA	2.797E-03	2.567E-03	NA
Mandible SA = 13881.4	Force/Mandible SA	7.098E-03	NA	6.379E-03
Psittacosaurus	m.AMES	133.200	71.503	58.614
	m.AMEP	90.150	48.393	39.670
	m.AMEM	64.800	34.785	28.515
	m.PSTs	99.750	53.546	43.894
	m.AMP	105.600	56.687	46.469
	m.PTd	17.400	9.340	7.657
	m.PTv	30.150	16.185	13.267
	TOTAL	**541.050**	**290.439**	**238.086**
Cranium SA = 113135	Force/Cranium SA	4.782E-03	2.567E-03	NA
Mandible SA = 37324.7	Force/Mandible SA	1.450E-02	NA	6.379E-03

Table S3: Muscle loads applied to the scaled models. Related to Figure 2. SA = surface area.

	Taxa														
	Heterodontosaurus			*Lesothosaurus*			*Scelidosaurus*			*Hypsilophodon*			*Psittacosaurus*		
Bite	**Pos.**	**Force**	**EFF**	**Pos.**	**Force**	**EFF**	**Pos.**	**Force**	**EFF**	**Pos.**	**Force**	**EFF**	**Pos.**	**Force**	**EFF**
Pred.	0	41.32	0.15	0	15.70	0.15	0	157.50	0.15	0	36.23	0.18	0	282.04	0.26
T1	0.23	50.51	0.18	0.27	21.58	0.21	0.12	178.00	0.17	0.29	46.35	0.24	0.56	406.61	0.38
T2	0.4	58.44	0.21	0.31	22.33	0.21	0.17	185.78	0.18	0.34	48.73	0.25	0.62	423.33	0.39
T3	0.43	60.70	0.22	0.35	22.76	0.22	0.22	193.18	0.19	0.38	51.28	0.26	0.69	441.04	0.41
T4	0.49	63.80	0.23	0.41	23.91	0.23	0.27	198.89	0.19	0.41	52.00	0.26	0.75	465.85	0.43
T5	0.56	67.20	0.25	0.49	25.33	0.24	0.31	213.06	0.21	0.49	55.34	0.28	0.81	489.49	0.45
T6	0.65	72.29	0.26	0.58	26.97	0.26	0.35	227.39	0.22	0.56	58.68	0.30	0.88	509.78	0.47
T7	0.73	76.31	0.28	0.65	28.82	0.28	0.38	231.06	0.22	0.62	63.61	0.32	0.94	545.15	0.50
T8	0.83	81.30	0.30	0.74	31.06	0.30	0.43	233.16	0.23	0.68	68.40	0.35	1	571.05	0.53
T9	0.92	85.01	0.31	0.82	33.57	0.32	0.48	254.48	0.25	0.75	74.44	0.38	NA	NA	NA
T10	1	86.20	0.32	0.9	36.48	0.35	0.52	269.64	0.26	0.82	80.38	0.41	NA	NA	NA
T11	NA	NA	NA	1	40.14	0.39	0.57	284.63	0.28	0.87	87.12	0.44	NA	NA	NA
T12	NA	NA	NA	NA	NA	NA	0.6	295.86	0.29	0.95	97.19	0.49	NA	NA	NA
T13	NA	NA	NA	NA	NA	NA	0.66	306.17	0.30	1	105.70	0.54	NA	NA	NA
T14	NA	NA	NA	NA	NA	NA	0.7	319.83	0.31	NA	NA	NA	NA	NA	NA
T15	NA	NA	NA	NA	NA	NA	0.76	342.98	0.33	NA	NA	NA	NA	NA	NA
T16	NA	NA	NA	NA	NA	NA	0.8	360.82	0.35	NA	NA	NA	NA	NA	NA
T17	NA	NA	NA	NA	NA	NA	0.85	371.59	0.36	NA	NA	NA	NA	NA	NA
T18	NA	NA	NA	NA	NA	NA	0.9	402.03	0.39	NA	NA	NA	NA	NA	NA
T19	NA	NA	NA	NA	NA	NA	0.93	408.08	0.40	NA	NA	NA	NA	NA	NA
T20	NA	NA	NA	NA	NA	NA	0.96	402.54	0.39	NA	NA	NA	NA	NA	NA
T21	NA	NA	NA	NA	NA	NA	1	404.14	0.39	NA	NA	NA	NA	NA	NA

Table S4: Unilateral bite forces outputted by finite-element models of the mandible. Related to Figure 2. Pred. = predentary bite, T*n* = bite at the *n*th tooth position. Pos. = the position of the bite position along the oral margin of the dentary, measured as its distance from the tip of the predentary divided by the total distance between the tip of the predentary to the posteriormost tooth. EFF = bite efficiency, measured as output bite force divided by total input muscle force.

	Taxa														
	Heterodontosaurus			*Lesothosaurus*			*Scelidosaurus*			*Hypsilophodon*			*Psittacosaurus*		
Bite	**Pos.**	**Force**	**EFF**	**Pos.**	**Force**	**EFF**	**Pos.**	**Force**	**EFF**	**Pos.**	**Force**	**EFF**	**Pos.**	**Force**	**EFF**
Pred.	0	42.28	0.15	0	15.94	0.15	0	158.14	0.15	0	36.36	0.18	0	281.15	0.26
T1	0.23	47.94	0.18	0.27	21.50	0.21	0.12	178.65	0.17	0.29	46.99	0.24	0.56	409.68	0.38
T2	0.4	59.26	0.22	0.31	22.13	0.21	0.17	187.67	0.18	0.34	49.83	0.25	0.62	437.02	0.40
T3	0.43	61.75	0.23	0.35	22.67	0.22	0.22	193.69	0.19	0.38	52.85	0.27	0.69	460.02	0.43
T4	0.49	65.48	0.24	0.41	24.03	0.23	0.27	202.18	0.20	0.41	53.64	0.27	0.75	486.65	0.45
T5	0.56	68.94	0.25	0.49	25.41	0.24	0.31	215.31	0.21	0.49	57.15	0.29	0.81	516.63	0.48
T6	0.65	75.55	0.28	0.58	26.94	0.26	0.35	223.76	0.22	0.56	60.24	0.31	0.88	539.49	0.50
T7	0.73	81.80	0.30	0.65	28.56	0.27	0.38	226.96	0.22	0.62	66.25	0.34	0.94	566.64	0.52
T8	0.83	89.33	0.33	0.74	30.73	0.30	0.43	238.34	0.23	0.68	71.78	0.36	1	603.77	0.56
T9	0.92	96.48	0.35	0.82	33.12	0.32	0.48	263.87	0.26	0.75	77.42	0.39	NA	NA	NA
T10	1	102.21	0.37	0.9	36.04	0.35	0.52	278.79	0.27	0.82	81.82	0.42	NA	NA	NA
T11	NA	NA	NA	1	39.34	0.38	0.57	294.12	0.28	0.87	90.16	0.46	NA	NA	NA
T12	NA	NA	NA	NA	NA	NA	0.6	308.22	0.30	0.95	101.53	0.52	NA	NA	NA
T13	NA	NA	NA	NA	NA	NA	0.66	314.24	0.30	1	109.65	0.56	NA	NA	NA
T14	NA	NA	NA	NA	NA	NA	0.7	341.59	0.33	NA	NA	NA	NA	NA	NA
T15	NA	NA	NA	NA	NA	NA	0.76	356.85	0.35	NA	NA	NA	NA	NA	NA
T16	NA	NA	NA	NA	NA	NA	0.8	385.66	0.37	NA	NA	NA	NA	NA	NA
T17	NA	NA	NA	NA	NA	NA	0.85	392.65	0.38	NA	NA	NA	NA	NA	NA
T18	NA	NA	NA	NA	NA	NA	0.9	433.38	0.42	NA	NA	NA	NA	NA	NA
T19	NA	NA	NA	NA	NA	NA	0.93	447.29	0.43	NA	NA	NA	NA	NA	NA
T20	NA	NA	NA	NA	NA	NA	0.96	461.92	0.45	NA	NA	NA	NA	NA	NA
T21	NA	NA	NA	NA	NA	NA	1	475.68	0.46	NA	NA	NA	NA	NA	NA

Table S5: Bilateral bite forces outputted by finite-element models of the mandible. Related to Figure 2. Bite forces calculated by summing those from both bite positions for a bilateral bite. Pred. = predentary bite, T*n* = bite at the *n*th tooth position. Pos. = the position of the bite position along the oral margin of the dentary, measured as its distance from the tip of the predentary divided by the total distance between the tip of the predentary to the

posteriormost tooth. EFF = bite efficiency, measured as output bite force divided by total input muscle force.